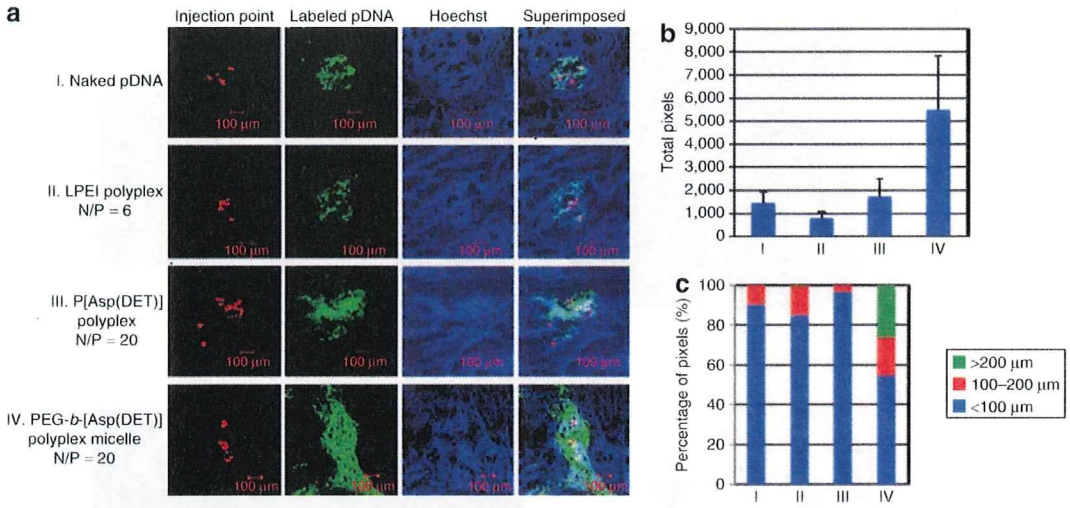

Figure 4 Intratumoral distribution of polyplexes and polyplex micelles after intratumoral injection. (**a**) Distribution of Cy3-labeled pDNA (green fluorescence) in a naked form or encapsulated into LPEI polyplexes (N/P = 6), P[Asp(DET)] polyplexes (N/P = 20), or PEG-*b*-P[Asp(DET)] polyplex micelles (N/P = 20) within human pancreatic adenocarcinoma BxPC3 tumors after intratumoral (i.t.) injection. The red and blue fluorescence are derived from fluorescent beads with a size of 15 μm as an indicator of injection point and Hoechst 33342 for the nuclear staining, respectively (more detailed data are shown in **Supplementary Figure S2**). (**b**) Total pixels and (**c**) percentage of pixels of fluorescent area of Cy3-labeled pDNA in three regions classified by the distance from the injection point. N/P, ratio of the number of amino groups units to a nucleotide unit.

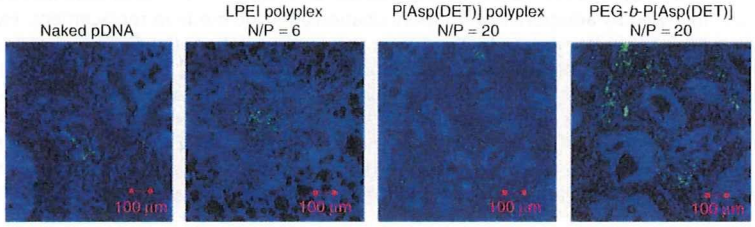

Figure 5 Gene expression of EGFP (green) within BxPC3 tumors at 6 days post-i.t. injection of naked plasmids, LPEI polyplexes (N/P = 6), P[Asp(DET)] polyplexes (N/P = 20), or PEG-b-P[Asp(DET)] polyplex micelles (N/P = 20). The blue fluorescence is derived from Hoechst 33342 for the nuclear staining. EGFP, enhanced green fluorescent protein; LPEI, linear polyethylenimine; N/P, ratio of the number of amino groups units to a nucleotide unit.

in **Figure 4b,c**, respectively. As a result, PEG-*b*-P[Asp(DET)] polyplex micelles showed a tendency to distribute more widely from the injection point compared with naked pDNA, LPEI and P[Asp(DET)] polyplexes. Note that irregular i.t. distribution of the polyplex micelles may be attributed to the heterogeneous structure of the BxPC3 tumors comprising clusters of dense tumor cells and interstitial tissues as indicated by the nuclear staining with Hoechst 33342.

In vivo gene expression after i.t. injection

The *in vivo* gene expression of fluorescent protein, enhanced green fluorescent protein (EGFP) within the BxPC3 tumors at 6 days post-i.t. injection of naked pDNA, LPEI polyplexes (N/P = 6), P[Asp(DET)] polyplexes (N/P = 20), or PEG-*b*-P[Asp(DET)] polyplex micelles (N/P = 20) was evaluated (n = 3). Note that P[Asp(DET)] polyplexes and polyplex micelles showed the highest transfection at 6 days postincubation in the MCTS models.[19] As shown in **Figure 5**, PEG-*b*-P[Asp(DET)] polyplex micelles apparently showed a widely distributed expression of EGFP in comparison with naked pDNA, LPEI, and P[Asp(DET)] polyplexes. These results seem to be consistent with the i.t. distribution of polyplex micelles (**Figure 4**).

Furthermore, the expression of hypoxia-responsive p5HRE + *Venus* within the BxPC3 tumors was evaluated (**Figure 6a**). The hypoxic region developed far from the vessels in the BxPC3 tumors was confirmed by fluorescein isothiocyanate-conjugated anti-Hypoxyprobe-1 monoclonal antibody (**Figure 6b**). Similar to **Figure 4c**, the pixels of fluorescent area in **Figure 6a** are classified into three different regions and summarized in **Figure 6c**. As a result, naked pDNA and LPEI polyplexes showed little gene expression, and P[Asp(DET)] polyplexes showed an appreciable gene expression in the region close to the injected point. In contrast, PEG-*b*-P[Asp(DET)] polyplex micelles showed well-distributed gene expression even in the furthest region from the injection point (>200 μm). These results suggest that the polyplex micelles might have the ability to percolate into the tumor tissue, thereby improving the gene transfection in the hypoxic regions of solid tumors.

DISCUSSION

Recently, we compared the transfection ability and cytotoxicity between P[Asp(DET)] polyplexes and PEG-*b*-P[Asp(DET)] polyplex micelles by using MCTS models.[19] We revealed that the PEGylation decreased the cytotoxicity of polyplexes without

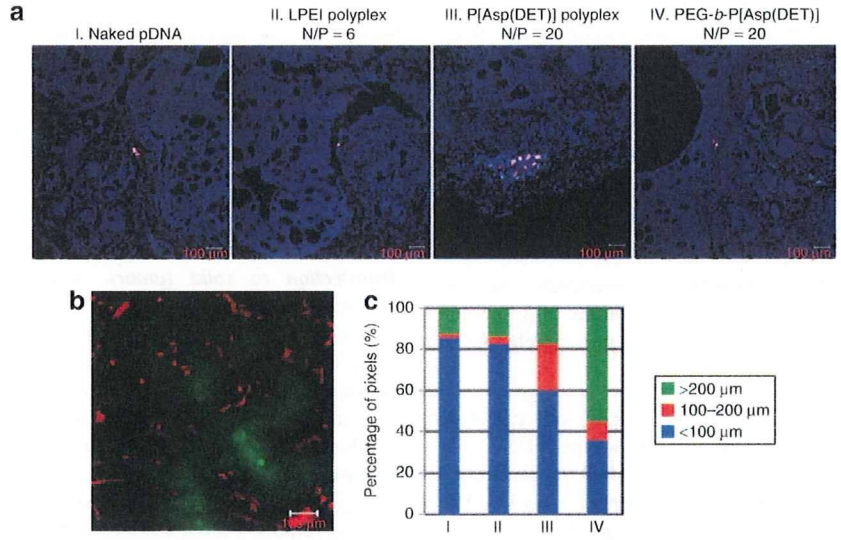

Figure 6 Hypoxia-responsive gene expression after intratumoral injection. (**a**) Gene expression of hypoxia-responsive p5HRE + *Venus* (white) within BxPC3 tumors at 6 days post-i.t. injection of naked plasmids, LPEI polyplexes (N/P = 6), P[Asp(DET)] polyplexes (N/P = 20), or PEG-b-P[Asp(DET)] polyplex micelles (N/P = 20). The red and blue fluorescence are derived from fluorescent beads with a size of 15 μm as an indicator of injection point and Hoechst 33342 for the nuclear staining, respectively. (**b**) Hypoxic regions in BxPC3 solid tumors. The red and green fluorescence are derived from anti-PECAM-1 antibody and anti-Hypoxyprobe-1 antibody, respectively. (**c**) Percentage of pixels of fluorescent area of transfected *Venus* protein in three regions classified by the distance from the injection point. i.t., intratumoral; LPEI, linear polyethylenimine; N/P, ratio of the number of amino groups units to a nucleotide unit.

compromising the transfection efficiency, while delaying the onset of gene expression. In this study, we report another important property of PEG-*b*-P[Asp(DET)] polyplex micelles, *i.e.*, tissue penetrability. We demonstrated that polyplex micelles showed facilitated percolation of loaded pDNA into the tumor tissue in both *in vitro* MCTS models and subcutaneous tumor models. Consequently, polyplex micelles showed a well-distributed gene expression after i.t. injection, allowing the transfection to the hypoxic regions of the tumors. These observations are in good agreement with our previous reports that polymeric micelles incorporating adriamycin showed enhanced percolation into the tumor tissue not only in the MCTS models[16] but also in subcutaneous tumors after intravenous administration.[17] Recently, Mellor *et al.* reported that cationic polyplexes from linear and branched PEI and lipoplexes showed penetration and transfection limited to the outer 3–5 proliferating cell layers in the large-sized MCTS (~474 nm).[11] Consistently, our results (**Figures 2b, 3d**, and **4–6**) also demonstrated not only *in vitro* but also *in vivo* that cationic polyplexes might show the limited penetration and localized transfection within the tumor. Furthermore, the result indicates for the first time that PEGylated polyplexes led loaded pDNA to show improved tissue penetrability compared with cationic polyplexes, exerting the appreciable gene expression in the inner hypoxia region.

PEGylation has apparently an advantage to prevent aggregation of polyplexes in the physiological condition with the presence of considerable amount of salt. Also, the PEGylation effectively masks the cationic nature of the core polyplexes, preventing nonspecific interaction serum proteins and extracellular matrices. Indeed, we observed that the PEG shielding of the P[Asp(DET)] polyplexes decreased the Zeta-potential from +30 mV to +6 mV. Such prevention of aggregate formation and reduced interaction with biological components by PEGylation may contribute to the facilitated percolation of the polyplexes into the tumor tissue. In this regard, the stability of polyplex micelles is an important issue during their penetration process into the tumor tissue. Our previous study revealed that the PEG-*b*-P[Asp(DET)] polyplex micelles showed much higher tolerability against the pDNA exchange reaction with an anionic lipid compared with the P[Asp(DET)] polyplexes.[19] Such increased stability of polyplex micelles is consistent with their improved penetration into the tumor tissue observed here. Furthermore, there are several reports that PEGylated nanoparticles show enhanced passage through the mucosal tissues to overcome intestinal barriers presumably due to the high flexibility and amphiphilicity of PEG chains.[21–23]

The detailed mechanisms of the enhanced percolation of polyplex micelles in the tumor tissue remain to be clarified yet; however, the results in this study clearly demonstrate that polyplex micelles might access the tumor cells in the hypoxic region with the intrinsic functions to deliver therapeutic genes. Thus, polyplex micelles are expected to treat hypoxic regions in the tumor tissue, potentially preventing the recurrence and malignant progression of solid tumors. Together with improved pharmacokinetic parameters, PEGylated polyplexes with a high tissue-percolation property might be promising nonviral vectors for *in vivo* cancer gene therapy.

MATERIALS AND METHODS

Plasmid DNA. The plasmid, pCAcc vector having CAG promoter,[24] was provided by RIKEN Bioresource Center (Ibaraki, Japan). Also, a fragment cDNA of SEYFP-F46L (*Venus*), which is a variant of yellow fluorescent protein with the mutation F46L,[25] was provided by A. Miyawaki at the Brain Science Institute, RIKEN and inserted into the pCAcc vector (pCAcc + *Venus*). Each pDNA was amplified in competent DH5α *Escherichia coli* and purified using HiSpeed Plasmid MaxiKit (Qiagen Sciences, Hilden, Germany). The plasmid, pGL5 vector having p5HRE, was provided by Faculty of Medicine, Kyoto University (Japan).[26] The DNA fragment encoding *Venus* was inserted between *Hind*III and *Xba*I sites of pGL3/5xHRE/CMVmp.

Nonviral vectors. LPEI (ExGen 500, 22 kd) was purchased from Fermentas (Burlington, Ontario, Canada). P[Asp(DET)] and PEG-*b*-P[Asp(DET)] were prepared as previously reported.[12–14] Briefly, β-benzyl-L-aspartate *N*-carboxyanhydride was polymerized by the initiation from the primary amino group of *n*-butylamine and MeO-PEG-NH_2 (M_w: 12,000) to obtain poly(β-benzyl L-aspartate) (PBLA) and PEG-*b*-PBLA, respectively. The degree of polymerization of PBLA was determined to be 98 for PBLA and 101 for PEG-*b*-PBLA by the ^1H NMR measurement. Then, PBLA and PEG-*b*-PBLA were reacted with diethylenetriamine (DET) (50 equiv to benzyl group of PBLA segment) under mild anhydrous conditions to obtain P[Asp(DET)] and PEG-*b*-P[Asp(DET)], respectively. The unimodal distribution and the almost 100% conversion of the BLA unit into Asp(DET) unit were confirmed by gel permeation chromatography and ^1H NMR measurements.

Preparation of polyplexes. Each polymer was mixed with pDNA in 10 mmol/l Tris–HCl (pH 7.4) at varying N/P ratios (final pDNA concentration: 100 μg/ml). Polyplex was applied to each well for transfection 30 minutes after preparation. Polyplex micelle was applied to each well for transfection after overnight incubation at ambient temperature.

Cell culture and preparation of MCTS. Human hepatoma HuH-7 cells (from JCRB Cell Bank, Osaka, Japan) and human pancreatic adenocarcinoma BxPC3 cells (from ATCC, Manassas, VA) were maintained in Dulbecco's modified Eagle's medium and RPMI 1640 medium, respectively, supplemented with 10% fetal bovine serum in a humidified atmosphere containing 5% CO_2 at 37 °C. MCTS were prepared by using the plate designed for spheroid formation (Sumiloncelltight; Sumitomo Bakelite, Tokyo, Japan) as reported previously.[15,18] The size of MCTS can be controlled by the incubation period. During the incubation, the medium was replaced by fresh medium containing 10% fetal bovine serum every 3 days.

Live/dead assay. Live and dead assay was accomplished with the Live/Dead kit protocol (Molecular Probes, Carlsbad, CA). MCTS was rinsed with PBS(−) and then incubated with a solution containing 0.8 μmol/l calcein AM [495 nm/515 nm (Ex/Em)] and 4 μmol/l EthD-1 (495 nm/635 nm) in PBS(−) for 3 hours at 37 °C, followed by the observation by LSM 510 confocal laser scanning microscope (CLSM) (Carl Zeiss).

Transfection to MCTS. MCTS was incubated for 6–8 days until the diameter became >400–500 μm. Then, each polyplex solution containing 1 μg pDNA was applied to each well for the transfection. After 24-hour incubation, the medium was replaced by fresh medium, followed by additional 24-hour incubation. The gene expression of the *Venus* or EGFP was then evaluated through the observation by CLSM.

Percolation of nonviral vectors into the MCTS. To visualize the distribution of nonviral vectors in MCTS, pDNA was labeled with Label IT Cy3 Labeling Kit (Mirus, Piscataway, NJ). In this experiment, MCTS with the diameter of 200–250 μm was incubated with polyplexes or polyplex micelles containing 1 μg Cy3-labeled pDNA for 24 hours. After 24-hour incubation, MCTS was harvested and rinsed, followed by observation by CLSM.

Animal models. BALB/c nude mice (female, 5 weeks old) were obtained from Charles River Laboratories (Tokyo, Japan). BxPC3 cells (5×10^6 cells in 100 μl of PBS) were injected subcutaneously into the BALB/c nude mice and allowed to grow for 2–3 weeks to reach the proliferative phase. All animal experimental protocols were performed in accordance with the policies of the Animal Ethics Committee of the University of Tokyo.

Percolation of nonviral vectors in solid tumors. After the tumor size reached 6–8 mm in a diameter, the mice received the i.t. injection of 2 μg Cy3-labeled pDNA in a naked or polyplex-encapsulated form [20 μl in 10 mmol/l HEPES buffer (pH 7.4)] by using the Hamilton Microliter Syringe (Hamilton, Reno, NV). In this experiment, 5 μl of FluoSpheres fluorescent microspheres (particle size: 15 μm, 645 nm/680 nm) were mixed with Cy3-labeled pDNA solution and simultaneously injected into the BxPC3 tumor for indication of the injection point. After 24 hours, the tumors were excised and fixed with 10% formalin and sucrose PBS(−), followed by freezing in dry-iced acetone. Frozen samples were sectioned at 10-μm thickness in a cryostat, and stained with Hoechst 33342 (Dojindo Laboratories, Tokyo, Japan). The fluorescent images were then observed by CLSM.

Transfection to solid tumors. According to the protocols for the percolation study, the tumor-bearing mice received the i.t. injection of 2 μg pCAcc + EGFP or p5HRE + *Venus* in a naked or polyplex-encapsulated form. The animals administered with pCAcc + EGFP were killed at 6 days postinjection, and the excised tumors were fixed as previously described. The fluorescence of frozen section of solid tumors was observed by CLSM. On the other hand, the animals administered with p5HRE + *Venus* were administered with Hypoxyprobe-1 (Millipore Chemicon, Billerica, MA) at 60 mg/kg via tail vein at 6 days postinjection, and then killed for removal of solid tumors. Frozen sections of the xenograft were stained with rat anti-PECAM-1 antibody (BD Pharmingen, Franklin Lakes, NJ), and subsequently stained with Alexa 594-conjugated anti-rat IgG antibody (Invitrogen Molecular Probes, Carlsbad, CA) and fluorescein isothiocyanate-conjugated anti-Hypoxyprobe-1 MAb. The section was further counter-stained with TOTO-3 (Invitrogen Molecular Probes), and the fluorescence images were captured by CLSM.

Quantitative analysis of fluorescent images. The pixels of fluorescent area of Cy3-labeled pDNA or transfected *Venus* protein in the tumor section were quantified by using the Image J software (http://rsb.info.nih.gov/ij/), and classified into three different regions by the distance from the injection point (<100 μm, 100–200 μm, >200 μm).

SUPPLEMENTARY MATERIAL

Figure S1. Distribution of labeled pDNA in BxPC3 MCTS transfected by each polyplex or polyplex micelles in intersectional profiles at the shown slices (Optical slice at the center of MCTS. Red fluorescence is Cy3 labeled-pDNA).

Figure S2. Distribution of Cy3-labeled pDNA (green fluorescence) in a naked form or encapsulated into LPEI polyplexes (N/P=6), P[Asp(DET)] polyplexes (N/P=20) or PEG-*b*-P[Asp(DET)] polyplex micelles (N/P=20) within human pancreatic adenocarcinoma BxPC3 tumors after the intratumoral injection.

ACKNOWLEDGMENTS

We thank Kotoe Date (the University of Tokyo) for technical assistance. This work was supported in part by the Core Research Program for Evolutional Science and Technology from Japan Science and Technology Agency.

REFERENCES

1. Boussif, O, Lezoualc'h, F, Zanta, MA, Mergny, MD, Scherman, D, Demeneix, B *et al.* (1995). A versatile vector for gene and oligonucleotide transfer into cells in culture and *in vivo*: polyethylenimine. *Proc Natl Acad Sci USA* **92**: 7297–7301.
2. Ogris, M and Wagner, E (2002). Targeting tumors with non-viral gene delivery systems. *Drug Discov Today* **7**: 479–485.
3. Merdan, T, Kopecek, J and Kissel, T (2002). Prospects for cationic polymers in gene and oligonucleotide therapy against cancer. *Adv Drug Deliv Rev* **54**: 715–758.
4. Pack, DW, Hoffman, AS, Pun, S and Stayton, PS (2005). Design and development of polymers for gene delivery. *Nat Rev Drug Discov* **4**: 581–593.
5. Erbacher, P, Roche, AC, Monsigny, M and Midoux, P (1995). Glycosylated polylysine/DNA complexes: gene transfer efficiency in relation with the size and the sugar substitution level of glycosylated polylysines and with the plasmid size. *Bioconjug Chem* **6**: 401–410.
6. Merdan, T, Callahan, J, Petersen, H, Kunath, K, Bakowsky, U, Kopecková, P *et al.* (2003). Pegylated polyethylenimine-Fab' antibody fragment conjugates for targeted gene delivery to human ovarian carcinoma cells. *Bioconjug Chem* **14**: 989–996.
7. Ogris, M, Brunner, S, Schüller, S, Kircheis, R and Wagner, E (1999). PEGylated DNA/transferrin-PEI complexes: reduced interaction with blood components, extended circulation in blood and potential for systemic gene delivery. *Gene Ther* **6**: 595–605.

8. Harada-Shiba, M, Yamauchi, K, Harada, A, Takamisawa, I, Shimokado, K and Kataoka, K (2002). Polyion complex micelles as vectors in gene therapy—pharmacokinetics and *in vivo* gene transfer. *Gene Ther* **9**: 407–414.
9. Jain, RK (2001). Delivery of molecular and cellular medicine to solid tumors. *Adv Drug Deliv Rev* **46**: 149–168.
10. Minchinton, AI and Tannock, IF (2006). Drug penetration in solid tumours. *Nat Rev Cancer* **6**: 583–592.
11. Mellor, HR, Davies, LA, Caspar, H, Pringle, CR, Hyde, SC, Gill, DR *et al.* (2006). Optimising non-viral gene delivery in a tumour spheroid model. *J Gene Med* **8**: 1160–1170.
12. Kanayama, N, Fukushima, S, Nishiyama, N, Itaka, K, Jang, WD, Miyata, K *et al.* (2006). A PEG-based biocompatible block catiomer with high buffering capacity for the construction of polyplex micelles showing efficient gene transfer toward primary cells. *ChemMedChem* **1**: 439–444.
13. Miyata, K, Oba, M, Nakanishi, M, Fukushima, S, Yamasaki, Y, Koyama, H *et al.* (2008). Polyplexes from poly(aspartamide) bearing 1,2-diaminoethane side chains induce pH-selective, endosomal membrane destabilization with amplified transfection and negligible cytotoxicity. *J Am Chem Soc* **130**: 16287–16294.
14. Akagi, D, Oba, M, Koyama, H, Nishiyama, N, Fukushima, S, Miyata, T *et al.* (2007). Biocompatible micellar nanovectors achieve efficient gene transfer to vascular lesions without cytotoxicity and thrombus formation. *Gene Ther* **14**: 1029–1038.
15. Itaka, K, Ohba, S, Miyata, K, Kawaguchi, H, Nakamura, K, Takato, T *et al.* (2007). Bone regeneration by regulated *in vivo* gene transfer using biocompatible polyplex nanomicelles. *Mol Ther* **15**: 1655–1662.
16. Bae, Y, Nishiyama, N, Fukushima, S, Koyama, H, Yasuhiro, M and Kataoka, K (2005). Preparation and biological characterization of polymeric micelle drug carriers with intracellular pH-triggered drug release property: tumor permeability, controlled subcellular drug distribution, and enhanced *in vivo* antitumor efficacy. *Bioconjug Chem* **16**: 122–130.
17. Kano, MR, Bae, Y, Iwata, C, Morishita, Y, Yashiro, M, Oka, M *et al.* (2007). Improvement of cancer-targeting therapy, using nanocarriers for intractable solid tumors by inhibition of TGF-beta signaling. *Proc Natl Acad Sci USA* **104**: 3460–3465.
18. Sutherland, RM (1988). Cell and environment interactions in tumor microregions: the multicell spheroid model. *Science* **240**: 177–184.
19. Han, M, Bae, Y, Nishiyama, N, Miyata, K, Oba, M and Kataoka, K (2007). Transfection study using multicellular tumor spheroids for screening non-viral polymeric gene vectors with low cytotoxicity and high transfection efficiencies. *J Control Release* **121**: 38–48.
20. An, WG, Kanekal, M, Simon, MC, Maltepe, E, Blagosklonny, MV and Neckers, LM (1998). Stabilization of wild-type p53 by hypoxia-inducible factor 1alpha. *Nature* **392**: 405–408.
21. Huang, Y, Leobandung, W, Foss, A and Peppas, NA (2000). Molecular aspects of muco- and bioadhesion: tethered structures and site-specific surfaces. *J Control Release* **65**: 63–71.
22. Samuel, KL, Elizabeth, OD, Harrold, S, Man, ST, Wang, Y, Cone, R *et al.* (2007). Rapid transport of large polymeric nanoparticles in fresh undiluted human mucus. *Proc Natl Acad Sci USA* **104**: 1482–1487.
23. Yoncheva, K, Guembe, L, Campanero, MA and Irache, JM (2007). Evaluation of bioadhesive potential and intestinal transport of pegylated poly(anhydride) nanoparticles. *Int J Pharm* **334**: 156–165.
24. Niwa, H, Yamamura, K and Miyazaki, J (1991). Efficient selection for high-expression transfectants with a novel eukaryotic vector. *Gene* **108**: 193–199.
25. Nagai, T, Ibata, K, Park, ES, Kubota, M, Mikoshiba, K and Miyawaki, A (2002). A variant of yellow fluorescent protein with fast and efficient maturation for cell-biological applications. *Nat Biotechnol* **20**: 87–90.
26. Harada, H, Kizaka-Kondoh, S and Hiraoka, M (2005). Optical imaging of tumor hypoxia and evaluation of efficacy of a hypoxia-targeting drug in living animals. *Mol Imaging* **4**: 182–193.

ARTICLE

Diffuse-Type Gastric Carcinoma: Progression, Angiogenesis, and Transforming Growth Factor β Signaling

Akiyoshi Komuro, Masakazu Yashiro, Caname Iwata, Yasuyuki Morishita, Erik Johansson, Yoshiko Matsumoto, Akira Watanabe, Hiroyuki Aburatani, Hiroyuki Miyoshi, Kunihiko Kiyono, Yo-taro Shirai, Hiroshi I. Suzuki, Kosei Hirakawa, Mitsunobu R. Kano, Kohei Miyazono

Background Diffuse-type gastric carcinoma is a cancer with poor prognosis that has high levels of transforming growth factor β (TGF-β) expression and thick stromal fibrosis. However, the association of TGF-β signaling with diffuse-type gastric carcinoma has not been investigated in detail.

Methods We used a lentiviral infection system to express a dominant-negative TGF-β type II receptor (dnTβRII) or green fluorescent protein (GFP) as a control in the diffuse-type gastric carcinoma cell lines, OCUM-2MLN and OCUM-12. These infected cells and the corresponding parental control cells were subcutaneously or orthotopically injected into nude mice. Angiogenesis was inhibited by infecting cells with a lentivirus carrying the gene for angiogenic inhibitor thrombospondin-1 or by injecting mice intraperitoneally with the small-molecule angiogenic inhibitor sorafenib or with anti-vascular endothelial growth factor (VEGF) neutralizing antibody (six or eight mice per group). Expression of phospho-Smad2 and thrombospondin-1 was investigated immunologically in human gastric carcinoma tissues from 102 patients. All statistical tests were two-sided.

Results Expression of dnTβRII into OCUM-2MLN cells did not affect their proliferation in vitro, but it accelerated the growth of subcutaneously or orthotopically transplanted tumors in vivo (eg, for mean volume of subcutaneous tumors on day 10 relative to that on day 0: dnTβRII tumors = 3.49 and GFP tumors = 2.46, difference = 1.02, 95% confidence interval [CI] = 0.21 to 1.84; $P = .003$). The tumors expressing dnTβRII had higher levels of angiogenesis than those expressing GFP because of decreased thrombospondin-1 production. Similar results were obtained with OCUM-12 cells. Expression of thrombospondin-1 in the dnTβRII tumor or treatment with sorafenib or anti-VEGF antibody reduced tumor growth, whereas knockdown of thrombospondin-1 expression resulted in more accelerated growth of OCUM-2MLN tumors than of GFP tumors (eg, mean tumor volumes on day 14 relative to those on day 0: thrombospondin-1–knockdown tumors = 4.91 and GFP tumors = 3.79, difference = 1.12, 95% CI = 0.80 to 1.44; $P < .001$). Positive association between phosphorylated Smad2 and thrombospondin-1 immunostaining was observed in human gastric carcinoma tissues.

Conclusions Disruption of TGF-β signaling in diffuse-type gastric carcinoma models appeared to accelerate tumor growth, apparently through increased tumor angiogenesis that was induced by decreased expression of thrombospondin-1.

J Natl Cancer Inst 2009;101:592–604

Gastric cancer is one of the most devastating human cancers, with approximately 880 000 new cases and 650 000 deaths worldwide per year (1,2). There are two types of gastric cancer: diffuse type and intestinal type. Diffuse-type gastric carcinoma, according to the Laurén classification (3), is highly metastatic and characterized clinically by rapid disease progression and poor prognosis (4). Although the incidence of intestinal-type gastric carcinoma has continuously decreased, the incidence of diffuse-type gastric carcinoma has increased progressively during the last 30 years, so that

Affiliations of authors: Department of Molecular Pathology and the Global Center of Excellence Program for "Integrative Life Science Based on the Study of Biosignaling Mechanisms," Graduate School of Medicine (AK, CI, YMo, EJ, YMa, KK, Y-tS, HIS, MRK, KM), Center for NanoBio Integration (MRK, KM), and Genome Science Division, Research Center for Advanced Science and Technology (AW, HA), University of Tokyo, Tokyo, Japan; Department of Surgical Oncology, Osaka City University Graduate School of Medicine, Osaka, Japan (MY, KH); Subteam for Manipulation of Cell Fate, Bio Resource Center, RIKEN, Tsukuba, Japan (HM).

Correspondence to: Kohei Miyazono, MD, Department of Molecular Pathology, Graduate School of Medicine, University of Tokyo, Hongo 7-3-1, Bunkyo-ku, Tokyo 113-0033, Japan (e-mail: miyazono-ind@umin.ac.jp).

See "Funding" and "Notes" following "References."

DOI: 10.1093/jnci/djp058

the diffuse type constitutes approximately one-third of all gastric carcinomas diagnosed in the United States (5). In contrast to the intestinal type, infection with *Helicobacter pylori* and chronic gastritis are often absent in the diffuse-type gastric carcinoma. Patients with diffuse-type gastric carcinoma often have thick stromal fibrosis with undifferentiated carcinoma cells scattered in the interstitium, which results in a stiff and thick gastric wall with reduced motility, but the tumors do not form ulcers or apparent mass lesions.

Transforming growth factor β (TGF-β) is a multifunctional cytokine that contributes to cancer progression by acting in both tumor cells and the tumor stroma (6). TGF-β binds to TGF-β serine–threonine kinase receptors type I and type II (TβRII) and transduces signals by phosphorylation of the receptor-regulated Smad2 and Smad3 proteins. Smad2 and Smad3 form complexes with Smad4, and these complexes regulate transcription of various target genes in the nucleus (7,8).

Because TGF-β is a potent inhibitor of epithelial cell proliferation, resistance to the inhibitory activity of TGF-β results in increased cell proliferation and cancer progression (9). Cancer cells in advanced tumors are often refractory to TGF-β–induced growth inhibition, and some tumors even increase their production of TGF-β ligands. TGF-β induces deposition of extracellular matrix in the tumor interstitium, which leads to fibrosis. TGF-β also induces perturbations of immune surveillance and regulates angiogenesis in vivo. Moreover, TGF-β may promote tumor growth by inducing epithelial cells to undergo the epithelial–mesenchymal transition (10,11), and inhibition of TGF-β signaling has been reported to prevent progression and metastasis of certain advanced tumors (12–15). In addition, decreased expression of TβRII, Smad2, and/or Smad4 or loss-of-function mutations in at least one of these genes has been observed in advanced stages of certain cancers, including colorectal cancer, breast cancer, and prostate cancer (16), and these changes in TGF-β signaling may affect progression of these cancers.

There is limited information regarding the role of TGF-β in diffuse-type gastric cancers. The thick stromal fibrosis observed in diffuse-type gastric carcinoma is induced by the TGF-β produced by cancer cells and by cancer-associated fibroblasts (17). Production of TGF-β1 has been reported to be associated with the progression of diffuse-type gastric carcinoma (18), although the relation of TGF-β1 expression to prognosis of gastric carcinoma is controversial (19). Disruption of TGF-β signaling by loss of Smad4 expression has also been observed in diffuse-type gastric carcinoma (20). However, detailed investigations on the roles of TGF-β signaling in diffuse-type gastric carcinoma have not been carried out. We therefore investigated the role of TGF-β signaling in diffuse-type gastric carcinoma by use of OCUM-2MLN and OCUM-12 cell lines and by disrupting TGF-β signaling.

CONTEXT AND CAVEATS

Prior knowledge

Diffuse-type gastric carcinoma has poor prognosis. Patients have high levels of transforming growth factor β (TGF-β) expression and thick stromal fibrosis.

Study design

The roles of TGF-β and thrombospondin-1, an angiogenic inhibitor that is regulated by TGF-β, were investigated in vitro studies in diffuse-type gastric carcinoma cell lines and in vivo studies in mouse models of diffuse-type gastric carcinoma and human diffuse-type gastric carcinoma tissue specimens from 102 patients.

Contribution

Growth of diffuse-type gastric carcinomas appeared to be accelerated by disruption of TGF-β signaling in mouse models (which may be analogous to what occurs during progression of this disease in humans), apparently because of increased tumor angiogenesis that was induced by decreased expression of thrombospondin-1.

Implications

Because loss of a receptor for TGF-β has been reported to induce tumor angiogenesis in various cancers, administration of angiogenesis inhibitors, such as sorafenib or thrombospondin-1 analogues, should be investigated as a treatment for cancers with disrupted TGF-β signaling pathways.

Limitations

Although mouse models of subcutaneous and orthotopic transplantation models were used, the experiments were conducted with immunocompromised mice. The growth of metastatic tumors was not investigated.

From the Editors

Patients, Materials, and Methods

Cell Lines

The OCUM-2MLN cell line was obtained from a lymph node metastasis of a mouse with orthotopically implantated OCUM-2M cells (21); the OCUM-2M line was originally established from a 49-year-old woman with diffuse-type gastric carcinoma (4). The OCUM-12 cell line was established from the peritoneal effusion of a 58-year-old man with diffuse-type gastric carcinoma that was diagnosed by endoscopy and histology. OCUM-12 cells were further confirmed to be tumorigenic in nude mice [(22) and M. Yashiro and K. Hirakawa, Osaka City University, unpublished data]. Both cell lines were cultured in Dulbecco's modified Eagle medium (DMEM) containing 10% fetal bovine serum, penicillin (100 U/mL), and streptomycin (0.1 mg/mL) (Invitrogen, Carlsbad, CA). To disrupt TGF-β signaling, we introduced a dominant-negative TGF-β type II receptor (dnTβRII) that lacks the intracellular kinase domain into the OCUM-2MLN and OCUM-12 cell lines (resulting in the 2MLN-dnTβRII and OCUM-12-dnTβRII cell lines, respectively) by use of a lentiviral infection system (23). We used the same lentivirus system to generate control OCUM-2MLN and OCUM-12 cells that expressed green fluorescent protein (GFP) (resulting in the 2MLN-GFP and OCUM-12-GFP cell lines, respectively) and OCUM-2MLN cells that expressed both dnTβRII and the angiogenic inhibitor thrombospondin-1 (resulting in the 2MLN-dnTβRII+TSP-1) (24,25). cDNAs for dnTβRII or for thrombospondin-1 were produced from mRNA extracted from the cultured OCUM-2MLN cell line by polymerase chain reaction (PCR). cDNAs encoding either dnTβRII with a carboxyl-terminal hemagglutinin epitope tag or thrombospondin-1 were inserted into the multicloning site of the lentiviral

vector pCSII-CMV-RfA by use of pENTR, according to the manufacturer's protocol (Invitrogen).

Antibodies and Reagents

The rabbit polyclonal antibodies against human and mouse phosphorylated Smad2 that were used for immunoblotting were a gift from A. Moustakas and C.-H. Heldin (Ludwig Institute for Cancer Research, Uppsala, Sweden). The rabbit monoclonal antibody against human and mouse phosphorylated Smad2 that was used for immunohistochemistry was from Millipore (Temecula, CA; clone A5S). The rat monoclonal antibody against mouse platelet–endothelial cell adhesion molecule-1 (PECAM-1) and mouse monoclonal antibody against human and mouse Smad2 and Smad3 (clone 18) were from BD (Franklin Lakes, NJ). The rat monoclonal antibody against hemagglutinin tag (clone 3F10) was from Roche (Basel, Swiss), and mouse monoclonal antibody against GFP (clone 1E4) was from Medical & Biological Laboratories, Co. (Woburn, MA). Mouse monoclonal antibody against human and mouse thrombospondin-1 was from Abcam (Cambridge, UK; clone A6.1). Alexa 488– and Alexa 594–conjugated secondary antibodies and the nuclear stain TOTO-3 for counterstaining were from Invitrogen Molecular Probes (Eugene, OR). TGF-β3 and TGF-β1, which show similar biological activities in vitro, were purchased from R&D Systems (Minneapolis, MN).

Immunoblot Analysis

We examined the expression of Smad2 and Smad3, phosphorylated Smad2, GFP, and hemagglutinin-tagged dnTβRII by immunoblot analyses in following cultured cells: 2MLN, 2MLN-GFP, 2MLN-dnTβRII, OCUM-12, OCUM-12-GFP, and OCUM-12-dnTβRII. These cells were lysed in a buffer containing 50 mM Tris–HCl (pH 8.0), 150 mM NaCl, 1% Nonidet P-40 (Nacalai Tesque, Kyoto, Japan), 5 mM EDTA, 0.5% deoxycholic acid sodium salt-monohydrate (Nacalai Tesque), 0.1% sodium dodecyl sulfate (SDS) (Nacalai Tesque), 1% aprotinin (Mitsubishi Pharma, Osaka, Japan), and 1 mM phenylmethylsulfonyl fluoride (Sigma, St Louis, MO). The cell lysates were boiled in SDS sample buffer (100 mM Tris–HCl at pH 8.8, 0.01% bromophenol blue, 36% glycerol, 4% SDS, and 10 mM dithiothreitol) and subjected to SDS–polyacrylamide gel electrophoresis. Proteins were electrotransferred from a polyacrylamide gel to Pall Fluorotrans-W membranes (Pall, East Hills, NY) and immunoblotted with antibodies. Bound antibodies were detected by use of an enhanced chemiluminescence detection system (Amersham Pharmacia Biotech, Piscataway, NJ). Each experiment was conducted two times, and a representative result is shown.

Cell Proliferation Assay

We cultured 2.5×10^4 2MLN, 2MLN-GFP, 2MLN-dnTβRII, or OCUM-12 cells per well in 12-well plates. On the next day (designated as day 0), some cultures were treated with TGF-β and control cultures were left untreated. Cells from duplicate cultures were counted as indicated with a hemocytometer. Each experiment was conducted two times, sample points were assayed in triplicate, and data were averaged. Data from one representative experiment of these are shown.

BALB/c Nude Mouse Model for Human Gastric Cancer

BALB/c nude male mice, aged 4–5 weeks, were obtained from Oriental Yeast Co. (Tokyo, Japan). All animal experimental protocols were performed in accordance with the policies of the Animal Ethics Committee of the University of Tokyo. A total of 5×10^6 cells in 100 μL of DMEM (n > 6 mice per group) was injected subcutaneously at the left flank of each mouse and allowed to grow for 1 week (for OCUM-2MLN cells) or 3 weeks (for OCUM-12 cells) when the major axis of the tumors was approximately 10 mm long. For the orthotopic transplantation model, a total of 5×10^6 cells in 50 μL of DMEM were injected into the gastric wall of each mouse (n = 8 mice per group) and allowed to grow for 1 week when tumor was approximately 5 mm in diameter.

Tumor Volume Measurement

The volume of subcutaneous xenograft tumors was measured externally every other day until the end of the evaluation period. Tumor volume was estimated by using the equation, $v = (ab^2)/2$, where v is volume, a is the length of the major axis of the tumor, and b is the length of its minor axis. The relative tumor volume was then calculated by dividing tumor volume on a given experimental day by that on day 0 (the day of initiation of treatment or evaluation). For orthotopic xenograft tumors, the tumor area on the gastric wall was measured by opening the abdomen on experimental day 14 and at the end of the evaluation period (day 21). The major and minor axes of tumors were measured with Adobe Photoshop software (Adobe Systems, Mountain View, CA), and tumor areas on the gastric wall were calculated with ImageJ software (National Institutes of Health, Bethesda, MD). Relative tumor area was obtained by dividing the area on day 21 by that on day 14.

RNA Isolation and Quantitative Real-Time Reverse Transcription-PCR

Total RNAs from gastric carcinoma cells or excised subcutaneous tumors were extracted with the RNeasy Mini Kit (QIAGEN, Valencia, CA). Sources of RNAs were as follows: cultured 2MLN, 2MLN-GFP, and 2MLN-dnTβRII cells at 0, 1, and 24 hours treated with TGF-β ligand at 1 ng/mL or left untreated (*see* Figure 1, B); cultured 2MLN-GFP and 2MLN-dnTβRII cells at 24 hours treated with TGF-β ligand at 1 ng/mL or left untreated, and subcutaneous tumors generated from these cells that were allowed to grow for 3 weeks in vivo (*see* Figure 2); cultured 2MLN-GFP, 2MLN-GFP+miTSP-1, and 2MLN-dnTβRII cells treated with TGF-β ligand at 1 ng/mL or left untreated, and subcutaneous tumors generated from these cells in vivo that were allowed to grow for 3 weeks (*see* Figure 4); and cultured OCUM-12-GFP and OCUM-12-dnTβRII cells at 24 hours treated with TGF-β ligand at 1 ng/mL or left untreated (*see* Figure 5). First-strand cDNAs were synthesized with the Quantitect Reverse Transcription kit (QIAGEN) with random hexamer primers. Quantitative real-time reverse transcription (RT)-PCR analysis was performed with the 7500 Fast Real-Time PCR system (Applied Biosystems, Foster City, CA) with the primers, as shown in Supplementary Table 1 (available online). Each experiment was conducted two times, each sample was assayed in triplicate, and data were averaged. Data from one representative experiment are shown.

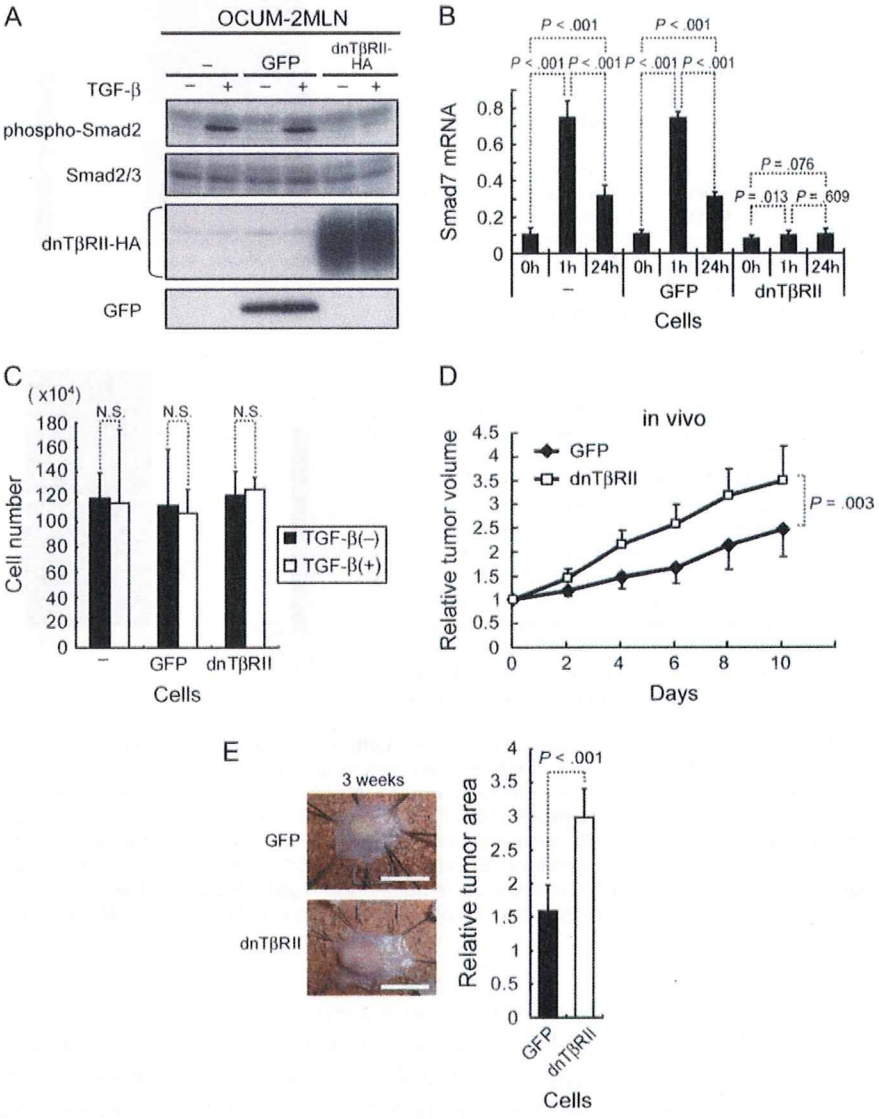

Figure 1. Disruption of TGF-β in gastric cancer cells and tumors. We used parental OCUM-2MLN cells, 2MLN cells expressing GFP (termed 2MLN-GFP cells) as a control, and 2MLN cells expressing a dnTβRII (termed 2MLN-dnTβRII cells). **A)** TGF-β signal transduction in the cells. Immunoblot analysis was used to compare the level of phosphorylated Smad2 (phospho-Smad2) with that of Smad2 and 3 as control, in parental OCUM-2MLN cells (**lanes –** = cells carry no constructs), 2MLN-GFP cells (**lanes GFP**), and 2MLN-dnTβRII cells (**lanes dnTβRII**), treated with TGF-β3 (1 ng/mL) or left untreated for 1 hour. Expression of dnTβRII protein (by use of hemagglutinin [HA] tag), and that of GFP, as a control for lentiviral infection was also determined by immunoblot analysis. The cells were subjected to immunoblot analysis with antibodies against the proteins indicated to the **left**. The experiment was conducted two times, and data from one representative experiment are shown. **B)** Human Smad7 mRNA expression. Quantitative real-time polymerase chain reaction was used to assess the level of expression of human Smad7 mRNA in all three cell lines after treatment with TGF-β3 (1 ng/mL), as indicated. The experiment was conducted two times, each sample was assessed in triplicate, and data were averaged. Data from one representative experiment are shown. **C)** Proliferation of gastric cancer cells in the presence of TGF-β3. Cells were treated with TGF-β3 (1 ng/mL) in 10% fetal bovine serum for 3 days; control cells were not treated with TGF-β3. The experiment was conducted two times, each sample was assessed in triplicate, and data were averaged. Data from one representative experiment are shown. **D)** Growth of 2MLN-GFP and 2MLN-dnTβRII tumors in nude mice for 10 days. Cells were subcutaneously transplanted into nude mice (n = 8 mice per group). **E)** Growth of orthotopic 2MLN-GFP and 2MLN-dnTβRII tumors in nude mice. Cells were transplanted into the gastric wall of nude mice (n = 8 mice per group). **Left)** Macroscopic appearance of representative samples of excised gastric wall with an orthotopic tumor. **Right)** Relative areas of the 2MLN-GFP and 2MLN-dnTβRII tumors. Scale bar = 10 mm. **Error bars** = 95% confidence intervals. All *P* values (two-sided) were calculated by using a Student's *t* test, except for that in (**D**), which was calculated by using a two-way repeated measures analysis of variance. dnTβRII = dominant-negative TGF-β type II receptor; GFP = green fluorescent protein; TGF-β = transforming growth factor β.

Microarray Analysis of Gene Expression in 2MLN-GFP or 2MLN-dnTβRII Tumors

Tissue samples from subcutaneous 2MLN-GFP or 2MLN-dnTβRII tumors were digested with collagenase (Worthington, Lakewood, NJ; 1 mg/mL) at 37°C for 1 hour, followed by treatment with 0.25% trypsin–EDTA (Invitrogen) at 37°C for 15 minutes. The resulting single-cell suspension was subjected to magnetic cell sorting (MACS®) with magnetic microbeads conjugated to CD326 antibody (Miltenyi Biotec, Auburn, CA) to separate CD326-positive human cancer cells from CD326-negative mouse stromal cells. Total RNAs from the isolated cancer cells were purified with the RNeasy Mini Kit (QIAGEN) and used for microarray analysis. Biotin-labeled complementary RNAs were synthesized and hybridized to the oligonucleotide microarray, GeneChip Human Genome U133 Plus2.0 (Affymetrix, Santa Clara, CA), according to Affymetrix technical manual. Gene expression data were normalized by use of the MAS5 algorithm according to the manufacturer's instruction. DAVID functional annotation clustering (26) with the Kyoto Encyclopedia of Genes and Genomes pathway database (http://genome.ad.jp/kegg/) was used for pathway analysis of the top 50 most variable probe sets of the GeneChip.

Histochemistry and Immunohistochemistry in Mouse Tissues

Excised mouse tissue samples were fixed for 1 hour in 10% neutral-buffered formalin at room temperature, washed overnight in phosphate-buffered saline containing 10% sucrose at 4°C, and embedded in optimal cutting temperature compound (Tissue-Tek; Sakura Finetek, Tokyo, Japan). Some samples were then snap frozen in a dry ice–acetone bath for immunohistochemistry, and other samples were fixed overnight in 4% paraformaldehyde and then embedded in paraffin for hematoxylin–eosin staining or AZAN staining to visualize collagen fibers. Frozen samples were

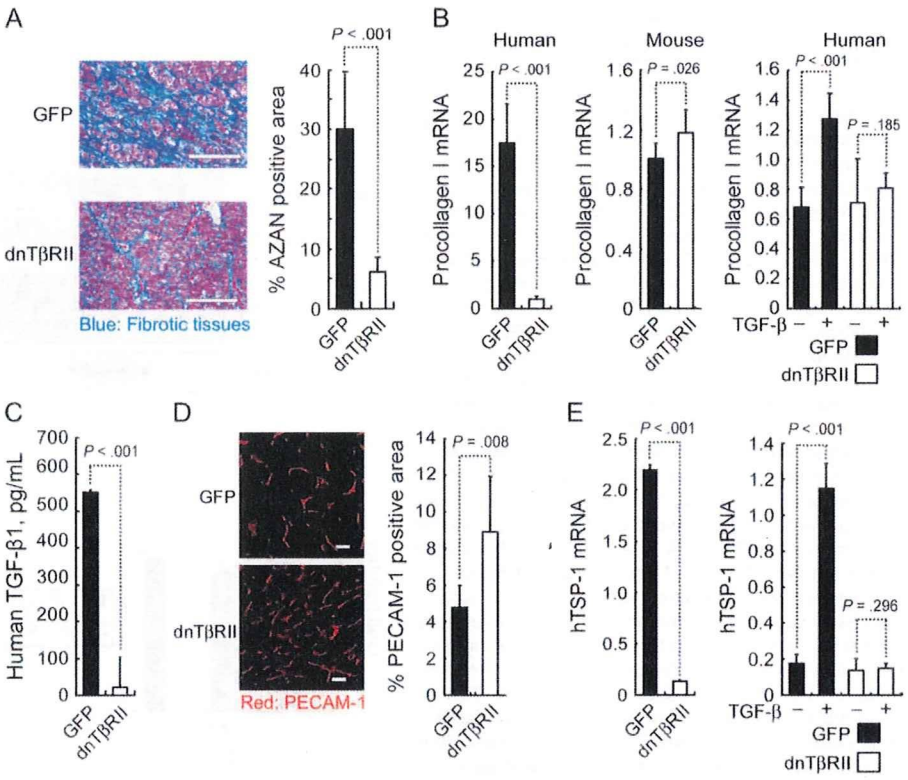

Figure 2. Histological characterization of 2MLN-GFP and 2MLN-dnTβRII xenograft tumors from nude mice. **A)** Fibrotic tissue in subcutaneous 2MLN-GFP (GFP) or 2MLN-dnTβRII (dnTβRII) xenograft tumors. **Left)** On day 14, fibrotic areas of tumor sections were visualized by AZAN staining and examined via light microscopy. Scale bars = 100 μm. **Right)** Quantification of fibrotic areas (n = 9 with each condition). **B)** Expression of human and mouse procollagen I mRNAs. **Left)** 2MLN-GFP subcutaneous tumors in nude mice. **Middle)** 2MLN-dnTβRII subcutaneous tumors in nude mice. **Right)** TGF-β treatment in 2MLN-GFP and 2MLN-dnTβRII cell lines. Cells were treated with TGF-β for 24 hours or left untreated (as indicated) and assayed for procollagen I mRNA with quantitative real-time polymerase chain reaction. Each experiment was conducted two times, each sample was assessed in triplicate, and data were averaged. Data from one representative experiment of these are shown. **C)** Concentrations of human TGF-β1 protein in 2MLN-GFP and 2MLN-dnTβRII cell culture supernatants. The level of TGF-β1 protein was determined by an enzyme-linked immunosorbent assay with an antibody specific for TGF-β1. The experiment was conducted two times, each sample was assessed in triplicate, and data were averaged. Data from one representative experiment of these are shown. **D)** Vascular density in 2MLN-GFP and 2MLN-dnTβRII xenograft tumors. Vascular density was determined by immunostaining with an antibody against PECAM-1 (n = 6 mice per group). **Left)** Micrographs of immunostained 2MLN-GFP and 2MLN-dnTβRII xenograft tumor sections. PECAM-1–positive areas are shown in **red** (n = 6 with each condition). Scale bars = 100 μm. **Right)** Percent PECAM-1–positive areas in 2MLN-GFP and 2MLN-dnTβRII xenograft tumor sections per microscopic field (n = 6 with each condition). **E)** Expression of hTSP-1 mRNA. **Left)** 2MLN-GFP and 2MLN-dnTβRII tumors in nude mice. **Right)** 2MLN-GFP and 2MLN-dnTβRII cells treated with TGF-β or left untreated for 24 hours in vitro, as indicated. Each experiment was conducted two times, each sample was assessed in triplicate, and data were averaged. Data from one representative experiment are shown. **Error bars** = 95% confidence intervals. All *P* values (two-sided) were calculated with a Student's *t* test. dnTβRII = dominant-negative TGF-β type II receptor; GFP = green fluorescent protein; TGF-β = transforming growth factor β; hTSP-1 = human thrombospondin-1; PECAM-1 = platelet–endothelial cell adhesion molecule-1.

further sectioned at a thickness of 10 μm with a cryostat, briefly fixed with 10% formalin, and then incubated with primary and secondary antibodies. Formalin-fixed samples of subcutaneous tumors and orthotopic tumors were subjected to hematoxylin–eosin and AZAN staining (*see* Figures 2, A and 4, C and Supplementary Figure 1, A, available online). Frozen samples of subcutaneous tumors were immunostained with anti-PECAM-1 and anti-rat Alexa 594 antibodies (*see* Figures 2, D and 4, B), or with anti-hemagglutinin and anti-rat Alexa 594 antibodies with TOTO-3 nuclear stain (*see* Figure 3, B). Frozen samples of orthotopic tumors were immunostained with anti-PECAM-1 and anti-rat Alexa 594 antibody (Supplementary Figure 1, B, available online).

Enzyme-Linked Immunosorbent Assay

Production of TGF-β1 by 2MLN-GFP and 2MLN-dnTβRII cells was determined with a sandwich enzyme immunoassay technique by using a Quantikine human TGF-β1 immunoassay (R&D Systems), according to the manufacturer's instruction. A total of 1×10^6 cells were cultured in 1% fetal bovine serum in six-well plates for 24 hours, and 100 μL of conditioned medium was removed and treated with 20 μL of 1 M HCl for 10 minutes, followed by neutralization with 20 μL of 1.2 M NaOH in 0.5 M HEPES (pH 7.4). Without this acidification step with 1 M HCl, levels of TGF-β1 in the conditioned medium could not be detected by the enzyme-linked immunosorbent assay. The samples were then pipetted into the wells of the microplate that had been precoated with a monoclonal antibody specific for TGF-β1 and incubated for 2 hours at room temperature. Subsequently, an enzyme-linked polyclonal antibody specific for TGF-β1 was added to the wells and incubated for additional 2 hours at room temperature to sandwich the TGF-β1 ligand. After a wash to remove unbound antibody–enzyme reagent, a substrate solution consisting of hydrogen peroxide and tetramethylbenzidine was added to the wells, and the intensity of the color developed was determined with a microplate reader (BIO-RAD, Hercules, CA). Each experiment was conducted two times, each sample point was assessed in triplicate, and data were averaged. Data from one representative experiment are shown.

Reduction of Thrombospondin-1 Expression by Use of MicroRNAs

The Block-iT Pol II miR RNAi expression system (Invitrogen) was used to knockdown the expression of thrombospondin-1. A microRNA construct against thrombospondin-1 was cloned into the pcDNA6.2-GW/EmGFP-mir vector (Invitrogen) after annealing the oligonucleotide 5′-AGAACTCAGTTACCATCTGCA-3′, which was designed to knockdown the expression of thrombospondin-1 by using BLOCK-iT RNAi Designer (Invitrogen). The EmGFP-miR thrombospondin-1 expression site was then inserted

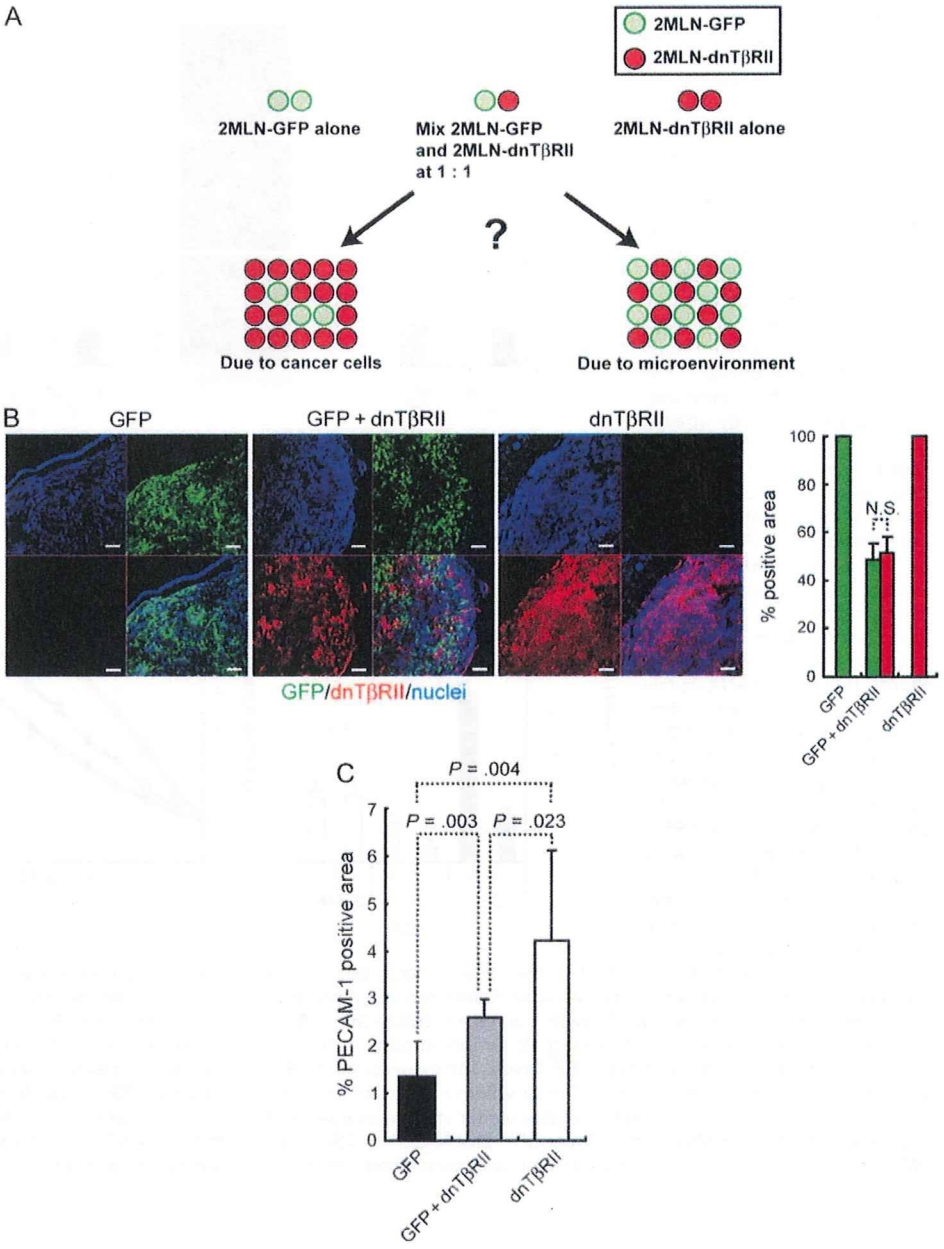

Figure 3. Characterization of xenograft tumors with a mixture of equal numbers of 2MLN-GFP (GFP) and 2MLN-dnTβRII (dnTβRII) cells. **A)** Developmental model of tumors inoculated with a mixture of 2MLN-GFP and 2MLN-dnTβRII. Equal amounts of the 2MLN-GFP and 2MLN-dnTβRII cells were mixed and transplanted into nude mice. The composition of tumors generated with a mixture of 2MLN-GFP and 2MLN-dnTβRII cells was compared with that of tumors generated with 2MLN-GFP or 2MLN-dnTβRII cells alone to investigate whether the tumor microenvironment serves as a major determinant of tumor growth. **B)** Distribution of 2MLN-GFP cells (GFP, **green**) and 2MLN-dnTβRII cells (as shown by a hemagglutinin tag that was detected with anti-hemagglutinin antibody, **red**) in mixed-cell tumors. 2MLN-GFP cells were identified by GFP fluorescence, and 2MLN-dnTβRII cells were identified by immunohistochemistry staining with an antibody specific for hemagglutinin and with nuclear counterstaining with TOTO-3. **Left)** Micrographs of sections from tumors generated with 2MLN-GFP cells alone, 2MLN-dnTβRII cells alone, or a mixture of both cell lines. Scale bars = 100 μm. **Right)** Percent hemagglutinin-positive areas and GFP-positive areas (n = 9 with each condition). **C)** Vascular areas in tumors generated with 2MLN-GFP cells alone, 2MLN-dnTβRII cells alone, or a mixture of both cell types. Vascular areas were identified by immunostaining with antibody against PECAM-1 (n = 3 in each condition). **Error bars** = 95% confidence intervals. All *P* values (two-sided) were calculated using the Student's *t* test. dnTβRII = dominant-negative TGF-β type II receptor; GFP = green fluorescent protein; TGF-β = transforming growth factor β; PECAM-1 = platelet–endothelial cell adhesion molecule-1.

into the pDONR221 vector (Invitrogen) by the BP recombination reaction according to the manufacturer's instructions, followed by its insertion into multicloning site of the lentiviral vector pCSII-EF-MCS LR recombination reaction (Invitrogen), according to the manufacturer's instruction. Stably transfected 2MLN-GFP cells, termed 2MLN-GFP+miTSP-1, in which the expression of thrombospondin-1 was silenced, were established by use of the lentiviral infection system by the methods as described above (23).

Treatment With Angiogenesis Inhibitors In Vivo

A small-molecule inhibitor of angiogenesis, sorafenib (Nexavar; Bayer Health Care, Leverkusen, Germany), was dissolved at 10 mg/mL in dimethyl sulfoxide as stock solution (ie, 5 mL of dimethyl sulfoxide was added to one-fourth of a 200-mg sorafenib tablet). An 80-μL aliquot of the sorafenib stock solution (800 μg of sorafenib) was diluted with 170 μL of phosphate-buffered saline to a final concentration of 3.2 mg/mL. One week after subcutaneous transplantation with 2MLN-GFP or 2MLN-dnTβRII cells or 4 weeks after subcutaneous transplantation with OCUM-12-GFP and OCUM-12-dnTβRII cells (n = 6 mice per group), sorafenib or a vehicle control was administered intraperitoneally to BALB/c nude mice every day. Fifty micrograms of anti-vascular endothelial growth factor (VEGF) neutralizing monoclonal antibody (MAB293; R&D Systems) (2.5 mg/kg) dissolved in 250 μL of phosphate-buffered saline to a concentration of 0.2 mg/mL or vehicle was intraperitoneally injected into these nude mice (n = 6 mice per group) twice a week for 14 days.

Immunohistochemistry of Human Gastric Cancer Tissues

We examined 102 consecutive surgical samples from patients with gastric cancer at the Osaka City University Hospital, Osaka, Japan,

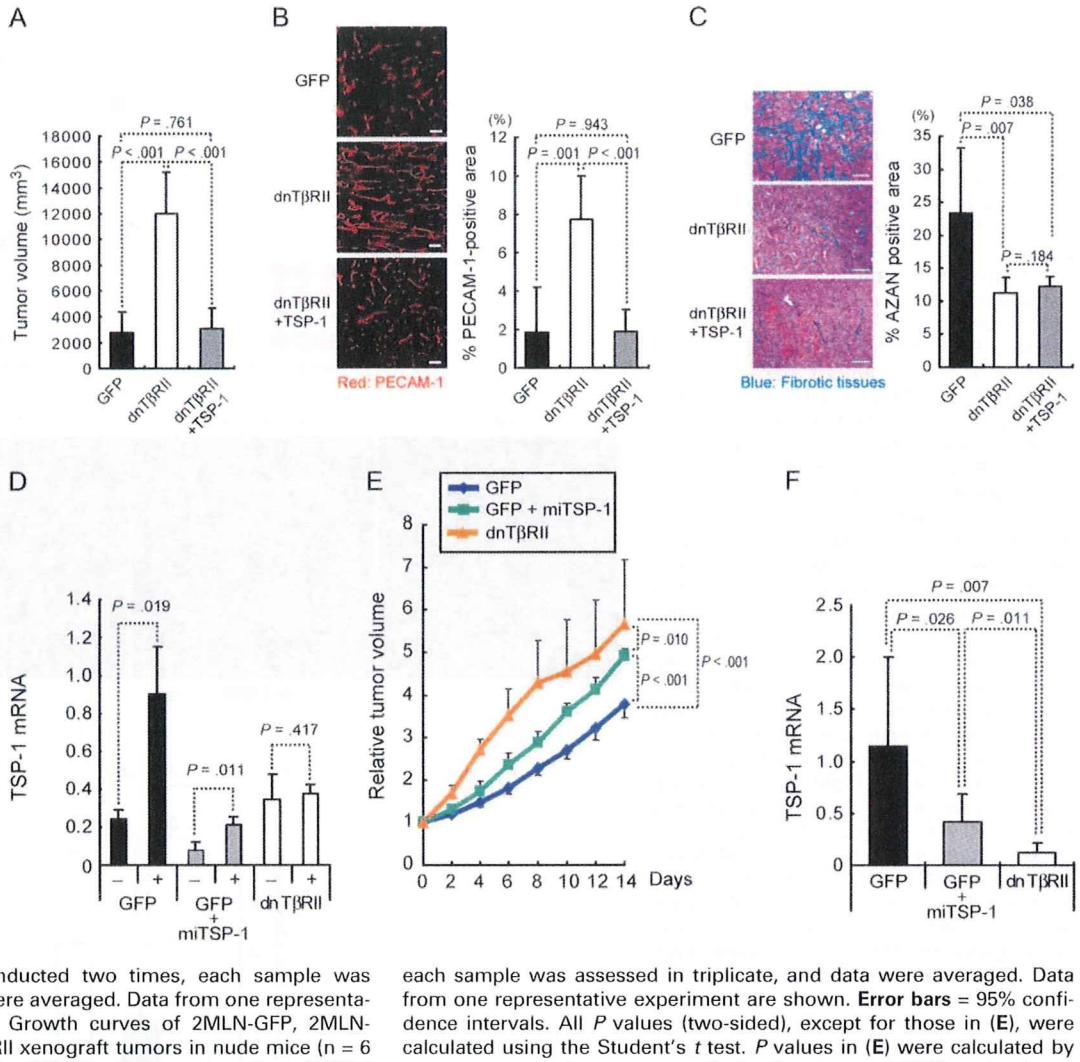

Figure 4. Expression of TSP-1 and tumor growth in nude mice. **A)** Tumor volume and TSP-1 expression. The 2MLN-dnTβRII cells, which stably express TSP-1, are termed 2MLN-dnTβRII+TSP-1. Volumes of the subcutaneous tumors produced by 2MLN-GFP, 2MLN-dnTβRII, and 2MLN-dnTβRII+TSP-1 cells were determined 7 days after inoculation (n = 6 mice per group). **B)** Vascular density at 7 days after inoculation as determined by immunostaining for PECAM-1. **Left)** Immunostaining with antibody against PECAM-1. Scale bars = 100 μm. **Right)** Percent PECAM-1–positive area (n = 3 with each condition). **C)** Fibrotic tissue as determined by AZAN staining in the subcutaneous tumors 7 days after inoculation. **Left)** Micrographs with fibrotic tissue stained **blue** by AZAN staining. Scale bars = 100 μm. **Right)** Percent AZAN-positive area (n = 3 with each condition). **D)** The effect of miTSP-1 mRNA expression in the gastric cancer cells as determined by TSP-1 mRNA expression. The 2MLN-GFP, 2MLN-GFP+miTSP-1, and 2MLN-dnTβRII cells were treated with TGF-β or left untreated for 24 hours in vitro, and expression of TSP-1 mRNA was compared among the cell lines. The experiment was conducted two times, each sample was assayed in triplicate, and data were averaged. Data from one representative experiment are shown. **E)** Growth curves of 2MLN-GFP, 2MLN-GFP+miTSP-1, and 2MLN-dnTβRII xenograft tumors in nude mice (n = 6 in each condition). In 2MLN-GFP+miTSP-1 cells, the expression of TSP-1 was reduced by use of the miTSP-1. Tumor volume is shown relative to the average volume in each condition at day 0 after starting evaluation. **F)** Expression of TSP-1 mRNA in the 2MLN-GFP, 2MLN-GFP+miTSP-1, and 2MLN-dnTβRII tumors in vivo. Experiment was conducted two times, each sample was assessed in triplicate, and data were averaged. Data from one representative experiment are shown. **Error bars** = 95% confidence intervals. All *P* values (two-sided), except for those in **(E)**, were calculated using the Student's *t* test. *P* values in **(E)** were calculated by two-way repeated measures analysis of variance. dnTβRII = dominant-negative TGF-β type II receptor; miTSP-1 = microRNA against thrombospondin-1; GFP = green fluorescent protein; TGF-β = transforming growth factor β; TSP-1 = thrombospondin-1; PECAM-1 = platelet–endothelial cell adhesion molecule-1.

which were obtained under a blanket written informed consent. Tissue sections were prepared from paraffin blocks and then incubated in antigen retrieval solution (Histo VT one; Nacalai Tesque, Kyoto, Japan) at 105°C for 20 minutes for thrombospondin-1 and for 40 minutes for phosphorylated Smad2. Sections were immunostained with primary and secondary antibodies. The primary antibodies used were rabbit anti-phosphorylated Smad2 monoclonal antibody and mouse anti-thrombospondin-1 monoclonal antibody. Secondary antibodies used were Alexa 488–conjugated goat anti-rabbit IgG antibody and/or Alexa 594–conjugated goat anti-mouse IgG antibody and were visualized by use of a Zeiss LSM510 Meta confocal microscope (Thornwood, NY) for immunohistochemistry and GFP fluorescence, and with an Olympus (Tokyo, Japan) AX80 microscope for hematoxylin–eosin and AZAN staining. Sections were scored positive when more than approximately 10% of the cancer cells were moderately or strongly stained, according to a recent study (27). In control experiments, the primary antibodies were omitted.

Statistical Analyses

Results were analyzed statistically by two-sided Student's *t* tests or by two-way repeated measures analysis of variance (ANOVA) tests with JMP6 software (SAS Institute, Raleigh, NC), where applicable. Results of immunohistochemistry for human surgical samples were analyzed with the χ^2 test. Results were considered to be statistically significant at $P < .05$. All statistical tests were two-sided.

Results

Disruption of TGF-β Signaling and Growth of Xenografted Tumors in Mice

We investigated the role of TGF-β signaling in human diffuse-type gastric carcinoma by transfecting OCUM-2MLN cells with lentiviral constructs expressing dnTβRIIs or a GFP control. We first determined whether the parental OCUM-2MLN cells and transfected 2MLN-GFP and 2MLN-dnTβRII cells respond to TGF-β in vitro by expressing GFP or dnTβRII, by use of

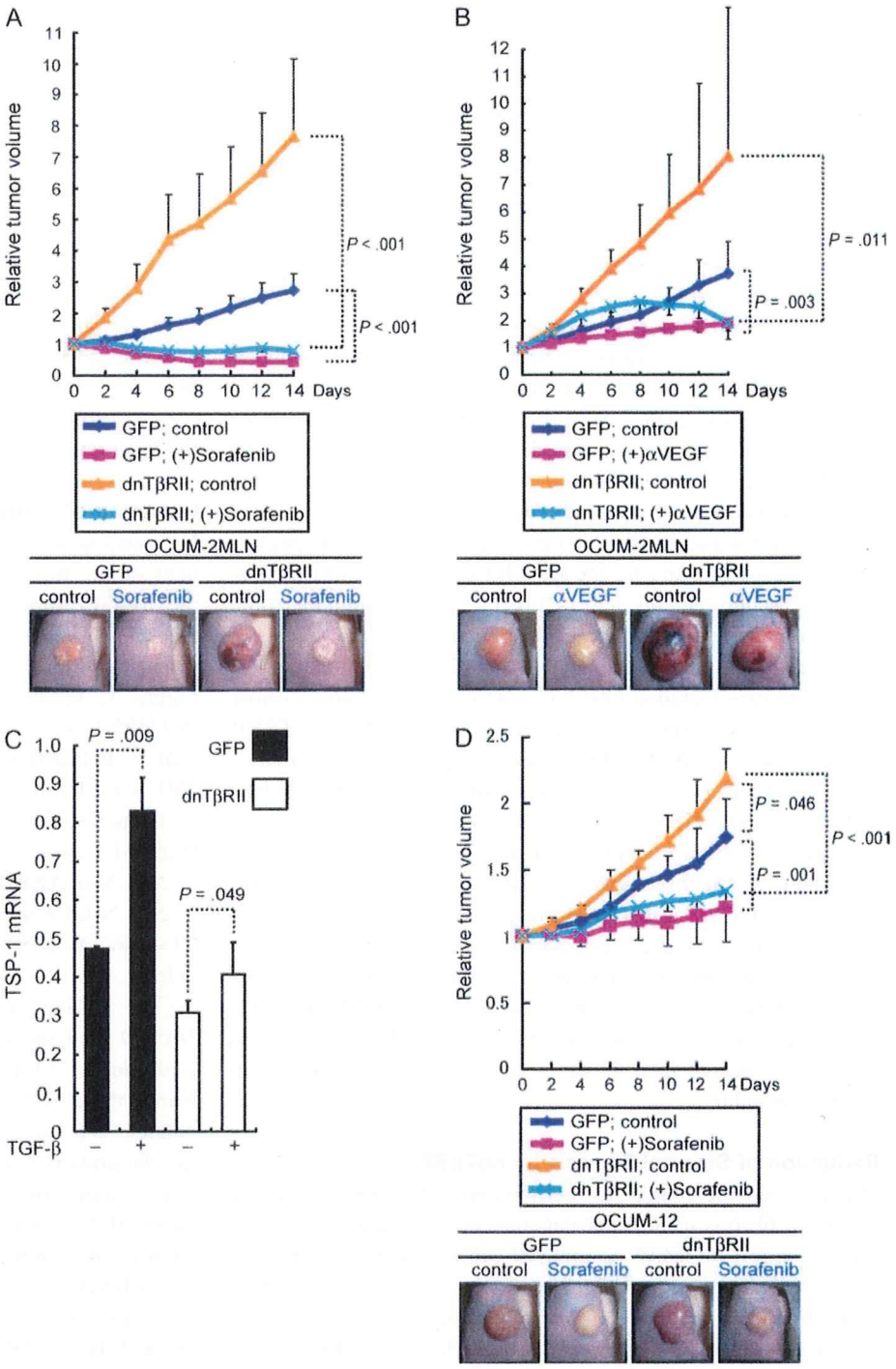

Figure 5. Administration of sorafenib and tumor growth in nude mice. **A)** Growth curve of xenografted 2MLN-GFP and 2MLN-dnTβRII tumors and sorafenib treatment. Mice bearing tumors were treated with 800 μg of sorafenib or with vehicle, as indicated, every day for 14 days (n = 6 mice per group). The representative macroscopic appearance of the tumors at day 7 is shown in the **bottom panels**. **B)** Growth curve of xenografted 2MLN-GFP and 2MLN-dnTβRII tumors in the presence and absence of anti-VEGF neutralizing antibody (n = 6 mice per group). Mice bearing tumors were treated for 14 days with 50 μg of anti-VEGF antibody or vehicle, as indicated, twice a week. The representative macroscopic appearance of the tumors at day 7 is shown in the **bottom panels**. **C)** Expression of human TSP-1 mRNA and treatment with TGF-β. TSP-1 mRNA expression was determined by quantitative real-time reverse transcription–polymerase chain reaction in the control OCUM-12-GFP (GFP) and OCUM-12-dnTβRII (dnTβRII) cells that were treated with TGF-β (1 ng/mL) or left untreated for 24 hours in vitro. The experiment was conducted two times, each sample was assessed in triplicate, and data were averaged. Data from one representative experiment of these are shown. **D)** Growth curves of xenografted OCUM-12-GFP and OCUM-12-dnTβRII tumors and sorafenib treatment. Mice bearing tumors were treated with 800 μg of sorafenib or with vehicle, as indicated, every day for 14 days (n = 7 mice per group). The representative macroscopic appearance of the tumors at day 14 is shown in the **bottom panels**. **Error bars** = 95% confidence intervals. *P* values for (**A**), (**B**), and (**D**) were calculated by two-way repeated measures analysis of variance. Those for (**C**) were calculated with a Student's *t* test, two-sided. DMSO = dimethyl sulfoxide (vehicle). dnTβRII = dominant-negative TGF-β type II receptor; GFP = green fluorescent protein; VEGF = vascular endothelial growth factor; TGF-β = transforming growth factor β; TSP-1 = thrombospondin-1.

immunoblotting. We found that GFP was expressed in the 2MLN-GFP control cells and dnTβRII was expressed in 2MLN-dnTβRII cells (Figure 1, A). In contrast to the parental 2MLN cells and GFP-transfected 2MLN-GFP cells, TGF-β–induced phosphorylated Smad2 was not detected in 2MLN-dnTβRII cells (Figure 1, A). We next used quantitative real-time RT-PCR analysis to show that the induction of Smad7 mRNA, a well-known target of TGF-β signaling, by TGF-β was lower in the 2MLN-dnTβRII cells than in OCUM-2MLN or 2MLN-GFP cells (Figure 1, B). 2MLN, 2MLN-GFP, and 2MLN-dnTβRII cells had similar proliferation rates, and the proliferation rates of these cells were not statistically significantly inhibited after TGF-β treatment (Figure 1, C).

Next, 2MLN-GFP or 2MLN-dnTβRII cells were subcutaneously transplanted into nude mice (n = 8 mice in each group), and tumor size was measured every other day until day 10. Although the proliferation of these cell types did not differ in vitro, the volumes of 2MLN-dnTβRII tumors were statistically significantly larger than those of 2MLN-GFP tumors (Figure 1, D; mean volume on day 10 relative to that on day 0 of 2MLN-dnTβRII tumors = 3.49 and of 2MLN-GFP tumors = 2.46, difference = 1.02, 95% confidence interval [CI] = 0.21 to 1.84; for group effect, $P = .003$;

and for the sampling time effect and the dnTβRII group effect × sampling time effect, $P < .001$, by a two-way repeated measures ANOVA test for tumor growth). We also orthotopically transplanted 2MLN-GFP or 2MLN-dnTβRII cells into the gastric wall of nude mice and determined tumor size on days 14 and 21 after implantation. The relative tumor area of 2MLN-dnTβRII (2.98) was statistically significantly larger than that of 2MLN-GFP (1.59) (Figure 1, E) (difference = 1.39, 95% CI = 0.87 to 1.91; $P < .001$, n = 8 mice in each group).

To explore factors responsible for the increased growth of the 2MLN-dnTβRII tumors in vivo, we used microarray analysis to identify differentially expressed human genes in the subcutaneously transplanted 2MLN-GFP and 2MLN-TβRII tumors and then used pathway analysis with the DAVID program to annotate the list of differentially expressed genes in these tumors. The DAVID program provides batch annotation and gene ontology term enrichment analysis to highlight the most relevant gene ontology terms associated with a given gene list (26). The analysis of our microarray data by the DAVID program identified three pathways as differentially activated pathways: cell communication, interactions between the extracellular matrix and the receptors, and focal adhesion (Supplementary Table 2, available online). All three pathways included *COL1A1*, *THBS1*, and *LAMC2*, whose expression levels were substantially lower in 2MLN-dnTβRII tumors than in 2MLN-GFP tumors (Supplementary Table 2, available online). *COL1A1* encodes procollagen I, which is involved in fibrosis, and *THBS1* encodes thrombospondin-1, which is an angiogenesis inhibitor. *LAMC2* encodes laminin-γ2 and was also included in all the three pathways. Although the increased expression of laminin-γ2 has been reported to be involved in invasion of certain cancers (28), the importance of its decreased expression in cancer remains unknown. Therefore, we further analyzed the relationship between the increased growth of the 2MLN-dnTβRII tumors and tumor microenvironment, especially fibrosis, with a focus on procollagen I, and angiogenesis, with a focus on thrombospondin-1.

Reduction of Stromal Fibrosis by dnTβRII

We analyzed the tumor microenvironment by determining the degree of fibrosis in the subcutaneous and orthotopic tumor tissues, as shown by AZAN staining of collagen fibers (Figure 2, A and Supplementary Figure 1, A, available online). In both tumor types, the area of fibrosis as determined by AZAN staining was statistically significantly lower in the 2MLN-dnTβRII tumors than in the 2MLN-GFP tumors (for subcutaneous tumors, 2MLN-dnTβRII had 6.1% and 2MLN-GFP had 30.1% [n = 9 mice per group], difference = 24.0%, 95% CI = 14.4% to 33.6%, $P < .001$; and for orthotopic tumors, 2MLN-dnTβRII tumors had 19.8% and 2MLN-GFP tumors had 47.0%, n = 9, difference = 27.2%, 95% CI = 20.0% to 34.4%, $P < .001$).

Microarray analysis revealed that the COL1A1 expression was lower in the 2MLN-dnTβRII tumors than in the 2MLN-GFP tumors. These results were validated with quantitative real-time RT-PCR with human COL1A1–specific primers and subcutaneous tumor samples (expression in 2MLN-dnTβRII tumors was 1.01 arbitrary units and that in 2MLN-GFP tumors was 17.46 arbitrary units, n = 3, difference = 16.4, 95% CI = 12.3 to 20.6 arbitrary units, $P < .001$) (Figure 2, B, left panel). In the same tumors, expression of the mouse Col1A1 mRNA was similar in 2MLN-dnTβRII and 2MLN-GFP tumors (Figure 2, B, middle panel; $P = .026$). In cultured cells, expression of the human COL1A1 mRNA was induced by TGF-β in the 2MLN-GFP cells but not in the 2MLN-dnTβRII cells (Figure 2, B, right panel). Secretion of TGF-β1 as determined by an enzyme-linked immunosorbent assay revealed that production of TGF-β1 was lower in 2MLN-dnTβRII cells (22.1 pg/mL) than in 2MLN-GFP cells (552.4 pg/mL) (difference = 530.3 pg/mL, 95% CI = 502.7 to 558.0 pg/mL, $P < .001$) (Figure 2, C). Thus, the material in the extracellular matrix in these tumors appears to be derived primarily from the gastric carcinoma cells and that the increased production of these extracellular matrix materials may be induced by TGF-β1 that is produced by the gastric carcinoma cells.

Induction of Tumor Angiogenesis by dnTβRII

We next examined tumor angiogenesis, another important component of the tumor microenvironment, in 2MLN-dnTβRII and 2MLN-GFP tumors in vivo. We used immunohistochemistry to determine vascular density in tumors with a specific marker of vascular endothelium, PECAM-1 (Figure 2, D and Supplementary Figure 1, B, available online). In subcutaneous tumors, the PECAM-1–positive area was statistically significantly higher in 2MLN-dnTβRII tumors (8.91% per microscopic field) than in 2MLN-GFP tumors (4.78%) (n = 6, difference = 4.13%, 95% CI = 1.31% to 6.94%; $P = .008$) (Figure 2, D). In orthotopic tumors, the PECAM-1–positive area was also statistically significantly higher in 2MLN-dnTβRII tumors (1.95% per microscopic field) than in 2MLN-GFP tumors (0.27%) (n = 7, difference = 1.67%, 95% CI = 0.46% to 2.88%; $P = .013$) (Supplementary Figure 1, B, available online).

The *THBS1* gene was included in all pathways selected by DAVID analysis, and the microarray analysis showed that the expression of THBS1 was lower in the 2MLN-dnTβRII tumors than in the 2MLN-GFP tumors (Supplementary Table 2, available online). We used quantitative RT-PCR with human THBS1–specific primers to confirm that the expression of THBS1 mRNA from human carcinoma cells was lower in the 2MLN-dnTβRII tumors (0.13 arbitrary unit) than in the 2MLN-GFP tumors (2.20 arbitrary units) (difference = 2.07 arbitrary units, 95% CI = 1.92 to 2.22 arbitrary units; $P < .001$) (Figure 2, E, left panel). Moreover, expression of thrombospondin-1 was potently induced by TGF-β in the 2MLN-GFP cells in vitro but not in the 2MLN-dnTβRII cells (Figure 2, E, right panel). In addition to thrombospondin-1, VEGF has been reported to be involved in angiogenesis in the Smad4-deficient pancreatic tumor model (29). However, the level of VEGF expression, as determined with primers specific for both human and mouse VEGF, was similar between 2MLN-GFP and 2MLN-dnTβRII cells in vivo and in vitro (data not shown), indicating that decreased expression of thrombospondin-1 may be involved in the enhanced angiogenesis in the 2MLN-dnTβRII tumors.

Phenotype of Tumors Containing a Mixture of Both 2MLN-GFP and 2MLN-dnTβRII Cells

The results described above strongly suggest that regulation of structural elements in the tumor microenvironment by TGF-β

signaling may be important to tumor formation in diffuse-type gastric carcinomas; however, it is still possible that the changes in tumor growth rate may be induced by other autonomous factor(s) in the cancer cells. To investigate further whether the tumor microenvironment serves as a major determinant of tumor growth in this model, we mixed equal amounts of the 2MLN-GFP and 2MLN-dnTβRII cells and transplanted the cell mixture into nude mice (Figure 3, A). If the tumor microenvironment plays a major role in tumor growth, then the 2MLN-GFP+dnTβRII tumors should contain equal number of both cell types (Figure 3, A). In contrast, if the 2MLN-dnTβRII portion of the tumor grows faster in cell-autonomous fashion, then the 2MLN-GFP+dnTβRII tumors should be composed mainly of 2MLN-dnTβRII cells. Histological examination of 2MLN-GFP+dnTβRII tumors with GFP fluorescence and by use of hemagglutinin antibody to detect the 2MLN-GFP and 2MLN-dnTβRII cells, respectively, revealed that the 2MLN-GFP+dnTβRII tumors contain almost equal number of the two cell types ($P = .56$) (Figure 3, B). We also examined angiogenesis in 2MLN-GFP+dnTβRII tumors by use of PECAM-1 immunostaining and found that the level of vascular density in the mixed-cell tumor (2.61% per microscopic field) was intermediate between that of 2MLN-dnTβRII tumors (4.22%) and 2MLN-GFP tumors (1.34%) (difference with 2MLN-dnTβRII tumors = 1.61, 95% CI = 0.37% to 2.86%, $P = .023$ [n = 3]; difference with 2MLN-GFP tumors = 1.27%, 95% CI = 0.73% to 1.81%, $P = .003$ [n = 3]) (Figure 3, C).

Inhibition of Angiogenesis and Growth of 2MLN-dnTβRII Tumors

To determine whether decreased thrombospondin-1 expression is involved in the accelerated proliferation of 2MLN-dnTβRII tumors, we used a lentivirus system to introduce the gene for thrombospondin-1 into the 2MLN-dnTβRII cells, and these cells were injected into mice to form tumors. At day 7, the volume of 2MLN-dnTβRII tumors that expressed exogenous thrombospondin-1 (3.08×10^3 mm^3) was lower than that of 2MLN-dnTβRII tumors alone (12.0×10^3 mm^3) (difference = 8.94×10^3 mm^3, 95% CI = 5.82×10^3 to 12.1×10^3 mm^3, $P < .001$ [n = 6]) and was similar to that of control 2MLN-GFP tumors that expressed GFP (2.81×10^3 mm^3; difference = 0.27×10^3 mm^3, 95% CI = -1.67×10^3 to 2.21×10^3 mm^3, $P = .76$ [n = 6]) (Figure 4, A). Immunostaining of the tumors with an antibody against PECAM-1 protein demonstrated that the vascular density of the 2MLN-dnTβRII tumors was reduced by the introduction of thrombospondin-1 (1.90% per microscopic field) compared with that of 2MLN-dnTβRII tumors alone (7.74%; difference = 5.84%, 95% CI = 4.21% to 7.48%, $P < .001$ [n = 3]) or that of 2MLN-GFP tumors as control (1.85% per microscopic field; difference = 0.05%, 95% CI = −1.64% to 1.73%, $P = .9$ [n = 3]) (Figure 4, B). In contrast, AZAN staining showed that the degree of fibrosis was not statistically significantly changed by introduction of thrombospondin-1 (Figure 4, C).

We obtained additional support for the finding that decrease in thrombospondin-1 is involved in the accelerated growth of the 2MLN-dnTβRII tumors by knocking down the expression of thrombospondin-1 in the 2MLN-GFP cells with an RNA interference approach. The 2MLN-GFP cells expressing the microRNA construct against thrombospondin-1 were termed 2MLN-GFP+miTSP-1 cells. Expression of thrombospondin-1 was lower in the 2MLN-GFP+miTSP-1 cells than in 2MLN-GFP cells in vitro (Figure 4, D). When these cells were inoculated to mice to form tumors, knockdown of thrombospondin-1 resulted in the volumes of 2MLN-GFP+miTSP-1 tumors being larger than those of 2MLN-GFP tumors (Figure 4, E; mean volume of 2MLN-GFP+miTSP-1 tumor on day 14 relative to that on day 0 after starting evaluation = 4.91 and that of 2MLN-GFP tumor = 3.79; difference = 1.12, 95% CI = 0.80 to 1.44; for group effect, sampling time effect, and group effect × sampling time effect, $P < .001$, by a two-way repeated measures ANOVA test for tumor growth [n = 6 in each group]). In addition, 2MLN-GFP+miTSP-1 tumors were smaller than 2MLN-dnTβRII tumors (Figure 4, E; volume of 2MLN-GFP+miTSP-1 tumor on day 14 relative to that on day 0 after starting evaluation = 4.91 and that of 2MLN-dnTβRII tumor = 5.65; difference = 0.74, 95% CI = −0.78 to 2.27; the result of a two-way repeated measures ANOVA test for the tumor growth from days 0 to 14 [n = 6 in each group] for group effect, $P = .010$; for sampling time effect, $P < .001$; for group effect × sampling time effect, $P = .025$), in agreement with the finding that the in vivo expression level of thrombospondin-1 mRNA in the 2MLN-GFP+miTSP-1 tumors (0.42) was higher than that of the 2MLN-dnTβRII tumors (0.12; difference = 0.30, 95% CI = 0.12 to 0.49; $P = .011$) (Figure 4, F).

To further elucidate the contribution of enhanced angiogenesis to increased tumor growth in the gastric carcinoma model, we treated the tumor-bearing mice with sorafenib, a small-molecule inhibitor of various tyrosine kinases, including VEGF receptor-2, Raf, and platelet-derived growth factor receptor (30,31). Sorafenib (40 mg/kg) or a vehicle control was intraperitoneally administered into the tumor-bearing mice every day (n = 6 mice per group). Treatment with sorafenib strongly suppressed the growth of both 2MLN-GFP tumors (Figure 5, A; tumor volume in treated mice on day 14 relative to that on day 0 after starting evaluation = 0.45 and that in untreated mice = 2.73; difference = 2.28, 95% CI = 1.81 to 2.76; for group effect, sampling time effect, and group effect × sampling time effect, $P < .001$, by a two-way repeated measures ANOVA test for tumor growth) and 2MLN-dnTβRII tumors (Figure 5, A; tumor volume in treated mice on day 14 relative to that on day 0 after starting evaluation = 0.79 and that in untreated mice = 7.64; difference = 6.85, 95% CI = 4.34 to 9.37; for group effect, sampling time effect, and group effect × sampling time effect, $P < .001$, by a two-way repeated measures ANOVA test for tumor growth). The tumors treated with sorafenib were pale in comparison with the untreated tumors, indicating the reduction of tumor vasculature and thus hemoglobin. To further confirm the effects of inhibition of angiogenesis on the tumor growth, an anti-VEGF neutralizing antibody (2.5 mg/kg) or a vehicle control was intraperitoneally administered into the tumor-bearing mice twice a week (n = 8 mice per group). As with sorafenib treatment, treatment with the anti-VEGF neutralizing antibody reduced the volume of both 2MLN-GFP tumors (Figure 5, B; tumor volume in treated mice on day 14 relative to that on day 0 after starting evaluation = 1.89 and that in control treated mice = 3.72; difference = 1.83, 95% CI = 0.68 to 2.98; for group effect, $P = .003$; and for sampling time effect and group effect × sampling time effect, $P < .001$, by a two-way repeated measures ANOVA test for tumor growth) and 2MLN-dnTβRII

tumors (Figure 5, B; tumor volume in treated mice on day 14 relative to that on day 0 after starting evaluation = 1.90 and that in control treated mice = 8.05; difference = 6.15, 95% CI = 0.12 to 12.18; for group effect, $P = .011$; and for sampling time effect and group effect × sampling time effect, $P < .001$, by a two-way repeated measures ANOVA test for tumor growth).

Disruption of TGF-β Signaling in Another Diffuse-Type Gastric Carcinoma Cell Line

In addition to OCUM-2MLN cells, we also used another diffuse-type gastric carcinoma cell line, OCUM-12, to investigate the effects of disruption of TGF-β signaling. TGF-β induced phosphorylation of Smad2 (Supplementary Figure 2, A, available online) and inhibited the proliferation of OCUM-12 cells in vitro (Supplementary Figure 2, B, available online), indicating that this cell line also responds to TGF-β. To further examine the effects of disrupting TGF-β signaling in this cell line, we generated OCUM-12 cells expressing GFP or dnTβRII and used them to confirm that phosphorylation of Smad2 was attenuated in OCUM-12-dnTβRII cells (Supplementary Figure 2, A, available online). We found that TGF-β1–induced thrombospondin-1 expression was attenuated in the OCUM-12-dnTβRII cells as it was in 2MLN-dnTβRII cells (Figure 5, C). Moreover, the volume of the OCUM-12 tumors expressing dnTβRII was statistically significantly larger than that of OCUM-12-GFP tumors (Figure 5, D; volume of OCUM-12-dnTβRII tumor on day 14 relative to that on day 0 after starting evaluation = 2.19 and that of OCUM-12-GFP tumor = 1.80; difference = 0.39, 95% CI = 0.014 to 0.772; for group effect, $P = .046$; for sampling time effect, $P < .001$; for group effect × sampling time effect, $P = .003$, by a two-way repeated measures ANOVA test for tumor growth [n = 7 mice in each group]), and sorafenib reduced the volume of both OCUM-12-GFP tumors (volume of treated tumor on day 14 relative to that on day 0 after starting evaluation = 1.17 and that of untreated tumor = 1.80; difference = 0.63, 95% CI = 0.28 to 0.98; for group effect, $P = .001$; and for sampling time effect and group effect × sampling time effect, $P < .001$, by a two-way repeated measures ANOVA test for tumor growth [n = 7 mice in each group]) and OCUM-12-dnTβRII tumors (volume of treated tumor on day 14 relative to that on day 0 after starting evaluation = 1.36 and that of untreated tumor = 2.19; difference = 0.83, 95% CI = 0.51 to 1.15; for group effect, $P < .001$; for sampling time effect and group effect × sampling time effect, $P < .001$, by a two-way repeated measures ANOVA test for tumor growth [n = 7 mice in each group]).

Expression of Thrombospondin-1 and Phosphorylated Smad2 in Human Gastric Carcinoma Tissues

Finally, we examined the status of TGF-β signaling in human gastric tumor tissues by use of antibody against phosphorylated Smad2 and the level of expression of thrombospondin-1 with antibody against thrombospondin-1. Both phosphorylated Smad2 and thrombospondin-1 were detected in normal epithelium adjacent to tumor (data not shown) and in some diffuse- and intestinal-type gastric cancer tissues (Supplementary Figure 3, A, available online). Immunostaining of 102 human gastric cancer specimens revealed that 44 (43%) tumors expressed both phosphorylated Smad2 and thrombospondin-1 and that 24 (23%) expressed neither (Supplementary Table 3, available online). Furthermore, a positive association was observed between the expression of thrombospondin-1 and of phosphorylated Smad2 ($P = .002$; Supplementary Table 3, available online). We also found that some cancer cells had weaker staining of phosphorylated Smad2 associated with weaker staining of thrombospondin-1 and that these cells were adjacent to cancer cells with strongly positive staining of phosphorylated Smad2 and strongly positive thrombospondin-1 (Supplementary Figure 3, B, available online). This observation suggested that the level of expression of thrombospondin-1 may be associated with the level of TGF-β signaling in each cancer cell, which varied even in the same tumor tissue.

Discussion

We demonstrated in this study that disruption of TGF-β signaling in diffuse-type gastric carcinoma models appears to accelerate the progression of cancer, as shown by increased growth of the 2MLN-dnTβRII tumors compared with that of the control 2MLN-GFP tumors in the subcutaneous and orthotopic transplantation models. Furthermore, microarray analysis of gene expression revealed decreased production of thrombospondin-1 in the 2MLN-dnTβRII tumors. Overexpression of thrombospondin-1 suppressed the growth of OCUM-2MLN tumors, but knockdown of thrombospondin-1 expression stimulated tumor growth. Moreover, we have also demonstrated that regulation of angiogenesis by sorafenib or anti-VEGF antibody efficiently prevented the growth of tumors in vivo.

Systemic administration of TGF-β inhibitors has been shown to suppress growth and metastasis of some tumors by acting on cancer cells and the tumor microenvironment (32,33). However, we found that disruption of TGF-β signaling in diffuse-type gastric carcinoma cells accelerated tumor formation. We found, in experiments with a mixture of the wild-type OCUM-2MLN cells and OCUM-2MLN cells expressing dnTβRII, that the increased growth of 2MLN-dnTβRII tumors appeared to be mainly attributable to alterations in the tumor microenvironment, not to autonomous properties of the cancer cells. The tumor microenvironment, which has been reported to be important during tumor progression (6), contains many structural elements, including blood vessels and fibrotic tissues. Consistently, we found that absence of TGF-β–induced expression of thrombospondin-1, an angiogenic inhibitor, is associated with increased growth of dnTβRII tumors in vivo, indicating that increased angiogenesis in the dnTβRII-expressing tumors appears to be important in the accelerated growth of such tumors.

TGF-β binds to TβRII and TGF-β type I receptorand activates Smad2 and Smad3, which transduce signals by complexing with Smad4. Decreased expression of TβRII, Smad2, and Smad4, or loss-of-function mutations in at least one of these genes, has been reported in various cancers at advanced stages, including breast cancer and colon cancer (16). Decreased expression of Smad4 has been observed in many clinical specimens of diffuse-type gastric carcinoma (20,34). Although mutations in TβRII have not been reported in diffuse-type gastric carcinoma, these findings indicate that disruption of TGF-β signaling may accelerate the progression of this type of cancer at advanced stages.

Schwarte-Waldhoff et al. (29) reported that the lack of Smad4 in an experimental pancreatic cancer model stimulated secretion of VEGF, repressed the expression of thrombospondin-1, and led to increased angiogenesis and tumor growth. Our microarray data revealed that although expression of VEGF was not statistically significantly altered in the 2MLN-dnTβRII tumors, compared with the 2MLN-GFP tumors, expression of thrombospondin-1 was reduced. Moreover, we found that the expression of thrombospondin-1 was induced by TGF-β in the OCUM-2MLN cells but not in the 2MLN-dnTβRII cells, in agreement with previous reports on the induction of thrombospondin-1 by TGF-β in certain cell types, including hepatic HuH-7 cells, osteosarcoma MG63 cells, and rat tubular epithelial cells (35,36). We obtained similar results with another diffuse-type gastric carcinoma cell line, OCUM-12. Furthermore, we found that expression of thrombospondin-1 reduced the growth of 2MLN-dnTβRII tumors in mice and that growth of tumors produced from 2MLN-GFP cells in which thrombospondin-1 expression had been inhibited was accelerated. Moreover, the association that we found between the expression of phosphorylated Smad2 and thrombospondin-1 indicated that attenuation or loss of TGF-β signaling results in decreased expression of thrombospondin-1 in human gastric cancer tissues. Thrombospondin-1 has been shown to inhibit growth and differentiation of endothelial cells and to induce their apoptosis (24,25). Thus, the decreased level of thrombospondin-1 in these tumor models appears to accelerate tumor angiogenesis.

The importance of tumor angiogenesis in the accelerated growth of the 2MLN-dnTβRII tumors was further supported by the potent inhibition of tumor growth by treatment with sorafenib, regardless of the status of TGF-β signaling in the cancer cells. Sorafenib was effective not only in OCUM-2MLN tumors but also in OCUM-12 tumors, although the latter were relatively resistant to sorafenib's growth inhibitory effect in vitro (A. Komuro, M. R. Kano and K. Miyazono, University of Tokyo, M. Yashiro and K. Hirakawa, Osaka City University, unpublished data; the 50% inhibitory concentration [IC_{50}] in OCUM-2MLN cells = 1.45 μM and in OCUM-12 cells = 8.75 μM). Thus, the effect of sorafenib on the gastric tumor models in vivo may be mostly due to suppression of tumor angiogenesis, although direct effects of sorafenib on the gastric carcinoma cells may also contribute to its growth inhibitory effect in vivo. In accordance with these results, we found that an anti-VEGF neutralizing antibody effectively reduced the growth of OCUM-2MLN tumors.

Our study had several limitations. Although we examined the growth of diffuse-type gastric carcinoma in subcutaneous and orthotopic transplantation models, the experiments were conducted with immunocompromised mice. Immune function may affect the growth of diffuse-type gastric carcinoma in human patients. Furthermore, we analyzed the growth of primary tumors but not the metastasis of tumors. The question of whether TGF-β signaling regulates metastasis in a cancer cell–autonomous fashion or in a microenvironment-dependent manner should be explored in the future.

In conclusion, we have shown that disruption of TGF-β signaling in a mouse model of diffuse-type gastric carcinoma, which may be analogous to what occurs during progression of this disease in humans, promotes tumorigenesis by accelerating angiogenesis. Because the loss of TβRII or Smad4 expression has been reported to induce tumor angiogenesis in other types of cancers (29,37), the administration of angiogenesis inhibitors, including sorafenib and thrombospondin-1 analogues (38), may be useful as a treatment for those cancers with disrupted TGF-β signaling pathways.

References

1. Crew KD, Neugut AI. Epidemiology of gastric cancer. *World J Gastroenterol.* 2006;12(3):354–362.
2. Hohenberger P, Gretschel S. Gastric cancer. *Lancet.* 2003;362(9380):305–315.
3. Laurén P. The two histological main types of gastric carcinoma: diffuse and so-called intestinal-type carcinoma. *Acta Pathol Microbiol Scand.* 1965;64:31–49.
4. Yashiro M, Chung YS, Nishimura S, Inoue T, Sowa M. Establishment of two new scirrhous gastric cancer cell lines: analysis of factors associated with disseminated metastasis. *Br J Cancer.* 1995;72(5):1200–1210.
5. Henson DE, Dittus C, Younes M, Nguyen H, Albores-Saavedra J. Differential trends in the intestinal and diffuse types of gastric carcinoma in the United States, 1973–2000. *Arch Pathol Lab Med.* 2004;128(7):765–770.
6. Bierie B, Moses HL. TGF-β and the tumor microenvironment. In: Derynck R, Miyazono K, eds. *The TGF-β Family.* New York, NY: Cold Spring Harbor Laboratory Press; 2008:965–987.
7. Feng XH, Derynck R. Specificity and versatility in TGF-β signaling through Smads. *Annu Rev Cell Dev Biol.* 2005;21:659–693.
8. Shi Y, Massagué J. Mechanisms of TGF-β signaling from cell membrane to the nucleus. *Cell.* 2003;113(6):685–700.
9. Roberts AB, Wakefield LM. The two faces of transforming growth factor β in carcinogenesis. *Proc Natl Acad Sci USA.* 2003;100(15):8621–8623.
10. Moustakas A, Heldin CH. Signaling networks guiding epithelial-mesenchymal transitions during embryogenesis and cancer progression. *Cancer Sci.* 2007;98(10):1512–1520.
11. Akhurst RJ. TGF-β signaling in epithelial-mesenchymal transition and invasion and metastasis. In: Derynck R, Miyazono K, eds. *The TGF-β Family.* New York, NY: Cold Spring Harbor Laboratory Press; 2008:939–964.
12. Yin JJ, Selander K, Chirgwin JM, et al. TGF-β signaling blockade inhibits PTHrP secretion by breast cancer cells and bone metastases development. *J Clin Invest.* 1999;103(2):197–206.
13. Muraoka RS, Dumont N, Ritter CA, et al. Blockade of TGF-β inhibits mammary tumor cell viability, migration, and metastases. *J Clin Invest.* 2002;109(12):1551–1559.
14. Yang YA, Dukhanina O, Tang B, et al. Lifetime exposure to a soluble TGF-β antagonist protects mice against metastasis without adverse side effects. *J Clin Invest.* 2002;109(12):1607–1615.
15. Azuma H, Ehata S, Miyazaki H, et al. Effect of Smad7 expression on metastasis of mouse mammary carcinoma JygMC(A) cells. *J Natl Cancer Inst.* 2005;97(23):1734–1746.
16. Lahn M, Berry B, Kloeker S, Yingling JM. TGF-β receptor kinase inhibitors for the treatment of cancer. In: ten Dijke P, Heldin CH, eds. *Smad Signal Transduction.* New York, NY: Springer Verlag; 2006:415–442.
17. Mizoi T, Ohtani H, Miyazono K, et al. Immunoelectron microscopic localization of transforming growth factor β1 and latent transforming growth factor β1 binding protein in human gastrointestinal carcinomas: qualitative difference between cancer cells and stromal cells. *Cancer Res.* 1993;53(1):183–190.
18. Kinugasa S, Abe S, Tachibana M, et al. Overexpression of transforming growth factor-β1 in scirrhous carcinoma of the stomach correlates with decreased survival. *Oncology.* 1998;55(6):582–587.
19. Vagenas K, Spyropoulos C, Gavala V, Tsamandas AC. TGFβ1, TGFβ2, and TGFβ3 protein expression in gastric carcinomas: correlation with prognostics factors and patient survival. *J Surg Res.* 2007;139(2):182–188.
20. Kim JY, Park DY, Kim GH, et al. Smad4 expression in gastric adenoma and adenocarcinoma: frequent loss of expression in diffuse type of gastric adenocarcinoma. *Histol Histopathol.* 2005;20(2):543–549.
21. Fujihara T, Sawada T, Hirakawa K, et al. Establishment of lymph node metastatic model for human gastric cancer in nude mice and analysis of factors associated with metastasis. *Clin Exp Metastasis.* 1998;16(4):389–398.

22. Qiu H, Yashiro M, Shinto O, Matsuzaki T, Hirakawa K. DNA methyltransferase inhibitor 5-aza-CdR enhances the radiosensitivity of gastric cancer cells. *Cancer Sci.* 2009;100(1):181–188.
23. Shibuya K, Shirakawa J, Kameyama T, et al. CD226 (DNAM-1) is involved in lymphocyte function-associated antigen 1 costimulatory signal for naive T cell differentiation and proliferation. *J Exp Med.* 2003;198(12):1829–1839.
24. Yamauchi M, Imajoh-Ohmi S, Shibuya M. Novel antiangiogenic pathway of thrombospondin-1 mediated by suppression of the cell cycle. *Cancer Sci.* 2007;98(9):1491–1497.
25. Jiménez B, Volpert OV, Crawford SE, Febbraio M, Silverstein RL, Bouck N. Signals leading to apoptosis-dependent inhibition of neovascularization by thrombospondin-1. *Nat Med.* 2000;6(1):41–48.
26. Dennis G Jr, Sherman BT, Hosack DA, et al. DAVID: Database for Annotation, Visualization, and Integrated Discovery. *Genome Biol.* 2003;4(5):P3.
27. Zhang J, Ito R, Oue N, et al. Expression of thrombospondin-1 is correlated with microvessel density in gastric carcinoma. *Virchows Archiv.* 2004;442(6):563–568.
28. Eguchi T, Inoue T, Fujii K, et al. Laminin-5 (gamma2 chain) is a marker of invading cancer cells in human gallbladder carcinoma: special emphasis on extension of carcinoma in situ along Rokitansky-Aschoff sinuses. *Oncol Rep.* 2008;20(1):33–39.
29. Schwarte-Waldhoff I, Volpert OV, Bouck NP, et al. Smad4/DPC4-mediated tumor suppression through suppression of angiogenesis. *Proc Natl Acad Sci USA.* 2000;97(17):9624–9629.
30. Wilhelm S, Carter C, Lynch M, et al. Discovery and development of sorafenib: a multikinase inhibitor for treating cancer. *Nat Rev Drug Discov.* 2006;5(10):835–844.
31. Liu L, Cao Y, Chen C, et al. Sorafenib blocks the RAF/MEK/ERK pathway, inhibits tumor angiogenesis, and induces tumor cell apoptosis in hepatocellular carcinoma model PLC/PRF/5. *Cancer Res.* 2006;66(24):11851–11858.
32. Nam JS, Terabe M, Mamura M, et al. An anti-transforming growth factor β antibody suppresses metastasis via cooperative effects on multiple cell compartments. *Cancer Res.* 2008;68(10):3835–3843.
33. Kawajiri H, Yashiro M, Shinto O, et al. A novel transforming growth factor β receptor kinase inhibitor, A-77, prevents the peritoneal dissemination of scirrhous gastric carcinoma. *Clin Cancer Res.* 2008;14(9):2850–2860.
34. Okano H, Shinohara H, Miyamoto A, Takaori K, Tanigawa N. Concomitant overexpression of cyclooxygenase-2 in HER-2-positive on Smad4-reduced human gastric carcinomas is associated with a poor patient outcome. *Clin Cancer Res.* 2004;10(20):6938–6945.
35. Okamoto M, Ono M, Uchiumi T, et al. Up-regulation of thrombospondin-1 gene by epidermal growth factor and transforming growth factor β in human cancer cells—transcriptional activation and messenger RNA stabilization. *Biochim Biophys Acta.* 2002;1574(1):24–34.
36. Nakagawa T, Lan HY, Glushakova O, et al. Role of ERK1/2 and p38 mitogen-activated protein kinases in the regulation of thrombospondin-1 by TGF-β1 in rat proximal tubular cells and mouse fibroblasts. *J Am Soc Nephrol.* 2005;16(4):899–904.
37. Lu SL, Herrington H, Reh D, et al. Loss of transforming growth factor-β type II receptor promotes metastatic head-and-neck squamous cell carcinoma. *Genes Dev.* 2006;20(10):1331–1342.
38. Ebbinghaus S, Hussain M, Tannir N, et al. Phase 2 study of ABT-510 in patients with previously untreated advanced renal cell carcinoma. *Clin Cancer Res.* 2007;13(22 Pt 1):6689–6695.

Funding

KAKENHI (Grant-in-Aid for Scientific Research; Project No. 17016011) from the Ministry of Education, Culture, Sports, Science, and Technology of Japan.

Notes

The study sponsors had no role in the design of the study or in the collection, analysis, or interpretation of the data. The authors take full responsibility for the study design, data collection, analysis and interpretation of the data, the decision to submit the manuscript for publication, and the writing of the manuscript.

We are grateful to Masako Oka for discussion, and Hiroko Yanagisawa, Makoto Arai, Saori Sakaue, and Satoru Yonekura for technical assistance.

Manuscript received August 6, 2008; revised January 28, 2009; accepted February 20, 2009.

Comparison of the effects of the kinase inhibitors imatinib, sorafenib, and transforming growth factor-β receptor inhibitor on extravasation of nanoparticles from neovasculature

Mitsunobu R. Kano,[1,2,3,4] Yukari Komuta,[1,5] Caname Iwata,[1] Masako Oka,[1] Yo-taro Shirai,[1] Yasuyuki Morishita,[1] Yasuyoshi Ouchi,[4] Kazunori Kataoka[2] and Kohei Miyazono[1,2,6]

[1]Department of Molecular Pathology, Graduate School of Medicine, University of Tokyo, 7-3-1 Hongo, Bunkyo-ku, Tokyo, 113-0033; [2]Center for Nano-Bio Integration, University of Tokyo, Tokyo, 113-8656; [3]Medical Scientist Training Program, Faculty of Medicine, University of Tokyo, Tokyo, 113-0033; [4]Department of Geriatrics, Graduate School of Medicine, University of Tokyo, 7-3-1 Hongo, Bunkyo-ku, Tokyo, 113-0033; [5]Japan Association for the Advancement of Medical Equipment, 3-42-6 Hongo, Bunkyo-ku, Tokyo, 113-0033, Japan

(Received May 20, 2008/Revised September 11, 2008/Accepted September 14, 2008/Online publication November 25, 2008)

There are a number of kinase inhibitors that regulate components of the neovasculature. We previously reported the use of transforming growth factor (TGF)-β inhibitor on neovasculature in stroma-rich tumor models to increase the intratumoral distribution of nanoparticles. Here, we compared the effects of two other kinase inhibitors, imatinib and sorafenib, with TGF-β inhibitor (LY364947) on extravasation of a modeled nanoparticle, 2 MDa dextran. We first used a mouse model of neoangiogenesis, the Matrigel plug assay, to compare neovasculature formed inside of and around Matrigel plugs (intraplug and periplug regions, respectively). Intraplug vasculature was more strongly pericyte covered, whereas periplug vasculature was less covered. In this model, TGF-β inhibitor exhibited the most potent effect on intraplug vasculature in increasing the extravasation of dextran, whereas sorafenib had the strongest effect on periplug vasculature. Although imatinib and TGF-β inhibitor each reduced pericyte coverage, imatinib also reduced the density of endothelium, resulting in a decrease in overall delivery of nanoparticles. These findings were confirmed in two tumor models, the CT26 colon cancer model and the BxPC3 pancreatic cancer model. The vasculature phenotype in the CT26 model resembled that in the periplug region, whereas the latter resembled that in the intraplug region. Consistent with this, sorafenib most potently enhanced the accumulation of nanoparticles in the CT26 model, whereas TGF-β inhibitor did in the BxPC3 model. In conclusion, the appropriate strategy for optimization of tumor vasculature for nanoparticles may differ depending on tumor type, and in particular on the degree of pericyte coverage around the vasculature. (*Cancer Sci* 2009; 100: 173–180)

The effectiveness of drug delivery into tumor tissues is an important issue in the treatment of solid tumors, in addition to the efficacy of drugs in treating tumor cells. For example, gemcitabine, a first-line anticancer agent for pancreatic adenocarcinoma, exhibited potent *in vitro* growth-inhibitory effects on a cultured cell line derived from the human pancreatic adenocarcinoma line BxPC3.[1] However, it exhibited only slight inhibitory effects on xenografted BxPC3 tumors in mice[2] and slight elongation of survival time in tumor-bearing patients, with significant effects only in the improvement of quality of life index in clinical trials.[3]

Many factors might potentially explain this discrepancy, particularly those related to tumor stroma.[4] Among them, tumor vasculature plays an important role in the delivery of anticancer agents. Extravasation of drugs to tumor tissue constitutes an essential part of drug delivery to tumor tissues,[5] whereas the molecular size of compounds is another important determinant of accumulation.[6] We have recently shown that increased leakiness in tumor neovasculature improves the accumulation of nanoparticles in tumor tissues in animal models of pancreatic adenocarcinoma and diffuse-type advanced gastric cancer.[7] In that study, inhibition of transforming growth factor (TGF)-β signaling reduced pericyte coverage and slightly increased endothelial area, resulting in an increase in vascular leakiness without loss of blood flow. However, numerous studies of tumor neovasculature have shown that it is leaky by nature, and that manipulation of vessels to make them less leaky, or induction of vascular normalization, may therefore benefit drug delivery to tumor tissues.[8] This theory has been supported with the use of vascular endothelial growth factor (VEGF) inhibitors. There are a number of VEGF inhibitors available, including neutralizing anti-VEGF antibodies such as bevacizumab (Avastin) and sorafenib (Nexavar). Sorafenib is a small molecular-weight (SMW) compound inhibiting multiple tyrosine kinases, including VEGF receptor (VEGFR) 2.[9]

The roles of pericytes in neoangiogenesis have also been well investigated.[10] Coverage of the neovasculature by pericytes stabilizes vascular structure.[11] Genetic ablation of platelet-derived growth factor (PDGF)-B signaling, one of the major signaling pathways in induction of pericyte maturation and recruitment to the endothelium, results in a bleeding tendency of the neovasculature.[11–13] PDGF-B signaling can be inhibited by the SMW inhibitor (SMWI) imatinib (Gleevec or Glivec), which inhibits the receptor for PDGF-B signaling, PDGF receptor (PDGFR) β, as well as PDGFRα and c-kit.[14] The use of imatinib along with VEGF inhibitors was shown to be effective in inhibiting tumor neovascularization in an animal model of spontaneous pancreatic islet tumor, the RIP-Tag model, through disruption of both pericytes and endothelium.[15]

Here we investigated the changes in vascular leakiness induced by three of the SMWI mentioned above, TGF-β inhibitor (LY364947), sorafenib, and imatinib, in the Matrigel plug assay as well as two animal cancer models. The Matrigel plug assay was carried out by mixing BD Matrigel Basement Membrane Matrix with VEGF-A, fibroblast growth factor (FGF)-2, and

[6]To whom correspondence should be addressed. E-mail: miyazono-ind@umin.ac.jp

doi: 10.1111/j.1349-7006.2008.01003.x

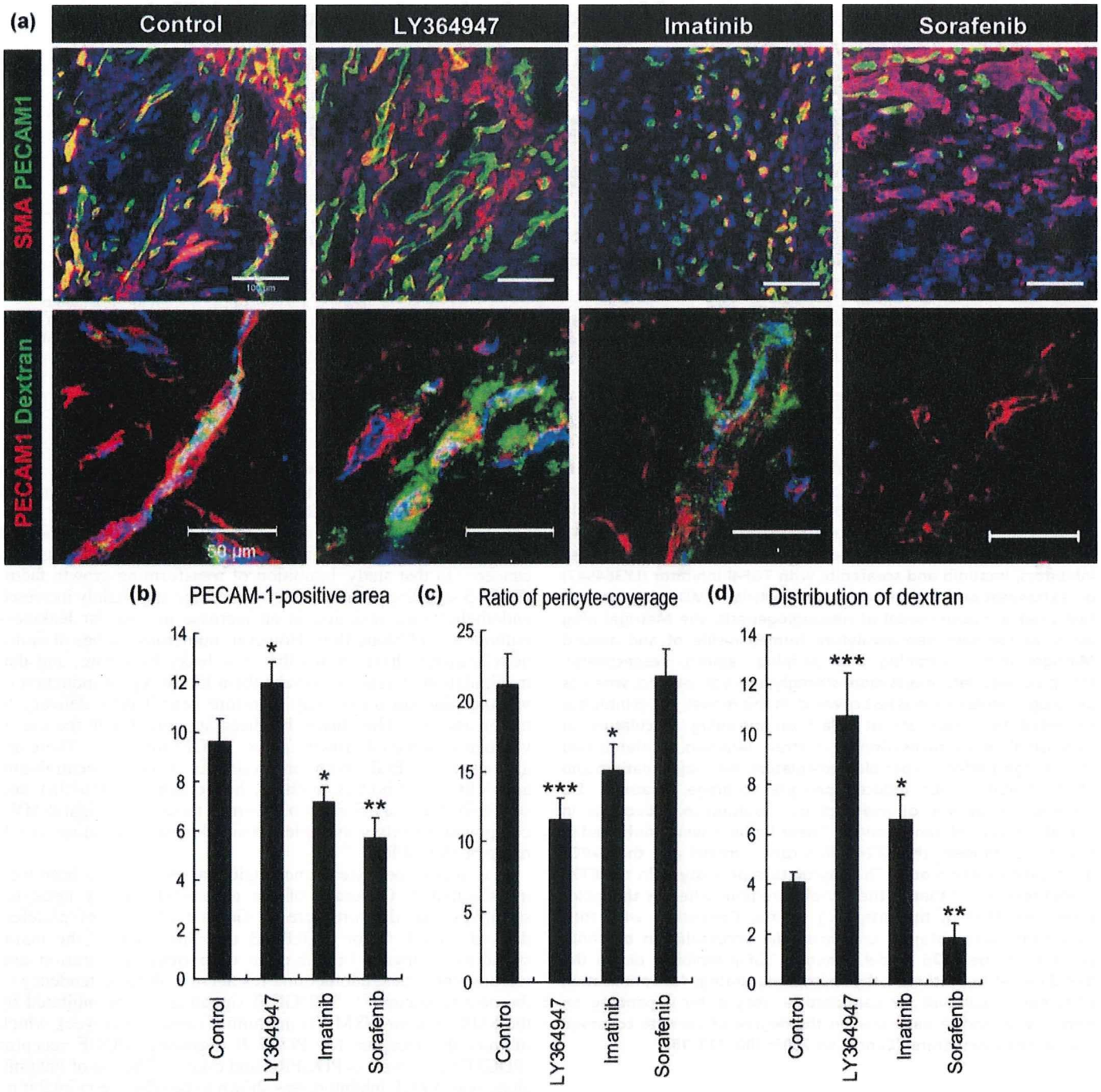

Fig. 1. The effects of three types of kinase inhibitors on extravasation of dextran in the Matrigel plug assay. (a) Confocal microscopy analyses. Upper row: staining of platelet endothelial cell adhesion molecule (PECAM)-1-positive endothelium in green and smooth muscle α-actin (SMA)-positive pericytes in red. Scale bars = 100 μm. Lower row: distribution of 2 MDa dextran in green and PECAM-1-positive endothelium in red. Scale bars = 50 μm. (b–d) Results of quantification (n = 15) of areas of endothelium (b, in percentage in one microscopic view), ratio of pericyte-covered endothelium (c, in percentage), and dextran distribution (d, in percentage in one microscopic view). Bars in the graphs represent standard errors. $^{*}P < 0.05$; $^{**}P < 0.01$; and $^{***}P < 0.001$.

heparin as angiogenic molecules to form mature neovasculature inside the gel plug, according to our previous report.[16] Of the two cancer models used in the present study, one was a well-established hypervascular cancer model using the murine colon cancer cell line CT26, whereas the other was an interstitium-rich cancer model using the human pancreatic cancer cell line BxPC3. With the latter model, we previously demonstrated therapeutic effects of combined use of TGF-β inhibitor on nanoparticles.[7] Using these models, we investigated the effects of SMWI on the distribution of 2 MDa dextran, a model of nanoparticles with an estimated hydrodynamic diameter of 50 nm.[6] The Matrigel plug assay and tumor model experiments revealed that TGF-β inhibitor increased extravasation of 2 MDa dextran in pericyte-covered neovasculature, whereas sorafenib increased that in vasculature with less pericyte coverage. These findings are important for determination of the optimal choice of angiogenic

doi: 10.1111/j.1349-7006.2008.01003.x

regulators in combination with nanoparticles for chemotherapy of cancer in general.

Materials and Methods

Reagents and antibodies. TGF-β inhibitor was purchased from Calbiochem (San Diego, CA, USA; LY364947, catalog no. 616451), imatinib was from Novartis Pharma (Tokyo, Japan), and sorafenib was from Bayer Healthcare (West Haven, CT, USA). These compounds were diluted in dimethyl sulfoxide to 5, 25, and 10 mg/mL, respectively, as stock solutions. Fluorescein isothiocyanate (FITC)-conjugated dextran of 2 000 000 Da (2 MDa) was obtained from Sigma-Aldrich (St Louis, MO, USA). The antibody to platelet endothelial cell adhesion molecule (PECAM)-1 was from BD PharMingen (San Diego, CA, USA), that to NG2 was from Chemicon (Temecula, CA, USA), and that to smooth muscle α-actin (SMA) (Cy3-conjugated) was from Sigma-Aldrich. AlexaFluor-conjugated secondary antibodies were purchased from Invitrogen Molecular Probes (Eugene, OR, USA).

Cancer cell lines and animals. The BxPC3 human pancreatic adenocarcinoma cell line was obtained from the American Type Culture Collection (Manassas, VA, USA), and was grown in RPMI-1640 medium supplemented with 10% fetal bovine serum. The murine colon adenocarcinoma CT26 cell line was from the National Cancer Center Research Institute, Japan, and was cultured in Dulbecco's modified Eagle's medium (Sigma-Aldrich) containing 10% fetal bovine serum. BALB/c mice and BALB/c nude mice, 5–6 weeks of age, were obtained from Sankyo Laboratory (Tokyo, Japan) and Charles River Laboratories (Tokyo, Japan), respectively.

***In vivo* Matrigel plug assay and cancer models.** Matrigel plugs were created by mixing 0.2 mg/mL recombinant human VEGF-A (VEGF165; R & D Systems, Minneapolis, MN, USA), 1 mg/mL FGF-2 (R & D Systems), and 0.1 mg/mL heparin (Aventis Pharma, Tokyo, Japan) by pipetting, in combination with regular Matrigel (catalogue no. 354234; BD Biosciences, Franklin Lakes, NJ, USA). Matrigel (400 μL per plug; one plug per mouse) was injected subcutaneously into the abdominal region of BALB/c mice. Each Matrigel plug was harvested on day 7 and frozen directly in dry-iced acetone for immunohistochemistry. As cancer models, 5×10^6 BxPC3 cells or 1×10^6 CT26 cells were implanted by subcutaneous injection into the abdominal region of BALB/c nude and normal BALB/c mice and allowed to grow for 3 weeks and 1 week, respectively, until reaching the proliferative phase. For the *in vivo* permeability assay, TGF-β inhibitor at 1 mg/kg, imatinib at 50 mg/kg, or sorafenib at 40 mg/kg was administered as one shot intraperitoneally 18 h before injection of dextran. Dextran was administered intravenously via lateral tail veins 6 h before harvesting of samples. For perfusion study in the tumor tissues, dextran of 2 MDa was administered intravenously, at 24 h after SMWI-administration and 10 min before harvesting, and the excised samples were directly fixed in formalin. All experimental protocols were carried out in accordance with the policies of the Animal Ethics Committee at the University of Tokyo.

Histology and immunohistochemistry. The excised samples were either directly frozen in dry-iced acetone for immunohistochemistry, or fixed overnight in 4% paraformaldehyde and then paraffin embedded to prepare them for hematoxylin–eosin (HE) staining or perfusion study in the tumor tissues. Frozen samples were further sectioned at 10 μm thickness in a cryostat, briefly fixed with 10% formalin, and then incubated with primary and fluorescent secondary antibodies. Samples were observed with a LSM510 Meta confocal microscope (Zeiss, Thornwood, NY, USA) for immunohistochemistry, and with an AX80 microscope (Olympus, Tokyo, Japan) for HE staining.

Quantification. Areas in Matrigel plugs that were PECAM-1-positive, double-positive for PECAM-1 and SMA, and FITC–dextran-positive in confocal micrographs ($n = 15$), or lengths of FITC–dextran-positive structure in the tumor tissues ($n = 12$) were measured using Adobe Photoshop software (Adobe Systems, San Jose, CA, USA) and ImageJ software (freeware distributed by the National Institutes of Health, USA). Pericyte coverage was quantified as the ratio of PECAM-1/SMA-double-positive areas to PECAM-1-positive areas, as described previously.[7] Results were further analyzed statistically by Student's *t*-test using Microsoft Excel software (Microsoft, Redmond WA, USA).

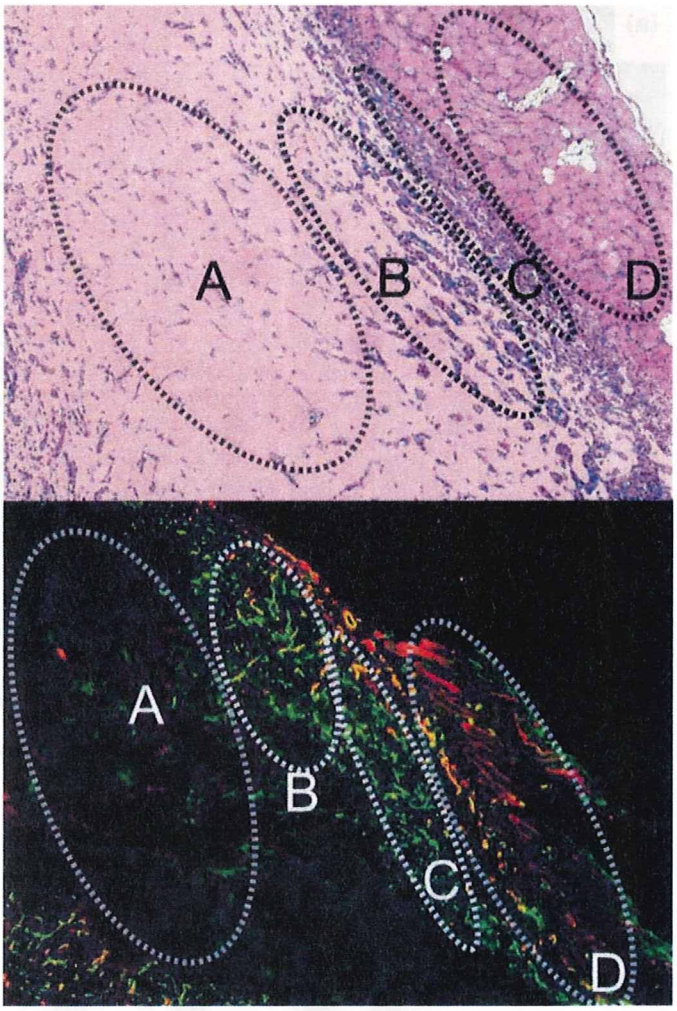

Fig. 2. Low-magnification view of the Matrigel plug and surrounding regions in sections with hematoxyline-eosin (HE) staining (upper) and with immunohistochemistry (lower). (a) Avascular area, (b) vascularized intraplug region, (c) periplug region, and (d) normal tissue. Green, platelet endothelial cell adhesion molecule-1; red, smooth muscle α-actin.

Results

We initially carried out the Matrigel plug assay *in vivo*, in which regular Matrigel was mixed with VEGF-A, FGF-2, and heparin[16] to investigate the effects of three SMWI on the extravasation of 2 MDa dextran (Fig. 1). Marked induction of pericyte-covered mature neovasculature was observed in the gel plug after a 7-day incubation in mice, as we reported previously.[16] Pericytes were determined to be SMA-positive cells in a Matrigel plug assay. In this model, administration of TGF-β inhibitor decreased pericyte coverage of the neovasculature and significantly enhanced the distribution of 2 MDa dextran. This observation was consistent